Mon. Not. R. Astron. Soc. **264,** 298–318 (1993)

VLA observations of a complete sample of core-dominated radio sources

D. W. Murphy,[1] I. W. A. Browne[2] and R. A. Perley[3]

[1] *Jet Propulsion Laboratory, MS 238-600, 4800 Oak Grove Drive, Pasadena, CA 91109, USA*
[2] *University of Manchester, Nuffield Radio Astronomy Laboratories, Jodrell Bank, Macclesfield, Cheshire SK11 9DL*
[3] *National Radio Astronomy Observatory, PO Box 0, Socorro, NM 87801, USA*

Accepted 1993 March 4. Received 1993 February 8

ABSTRACT

Maps with high dynamic range are presented of a well-defined sample of powerful core-dominated radio sources, all of which have 5-GHz core flux densities >1 Jy. The maps were made at a frequency of 1.64 GHz from combined VLA A and B configuration data. A novel technique for producing high dynamic range maps of variable sources from data taken at different epochs is described.

It is found that, on average, BL Lac objects are not more core-dominated than the quasars in the sample. This provides no support for the view that BL Lacs are those quasars seen at such small angles to the line of sight that their relativistically beamed core emission swamps that from other components. The results are consistent with most BL Lac objects being the beamed cores of low-luminosity (FRI) radio galaxies. Nevertheless, a substantial fraction of BL Lac objects, especially those with redshifts >0.5, have extended radio emission whose luminosity is equivalent to that of high-luminosity (FRII) radio galaxies. The existence of these objects has serious implications for 'unified schemes'.

Amongst the broad-line objects we find no evidence that those classified as highly polarized or optically violently variable are any more core-dominated than the rest.

Key words: methods: data analysis – BL Lacertae objects: general – quasars: general – radio continuum: galaxies.

1 INTRODUCTION

Much attention has been focused in recent years on determining whether apparently different classes of active galactic nuclei (AGN) are intrinsically different, or whether they result from viewing similar objects in different orientations. An excellent review of the subject was given by Lawrence (1987). Attempts to class as one objects thought previously to be intrinsically different have become known as unified schemes. One unified scheme of particular interest to radio astronomers is the proposal that the two types of radio-loud quasar, the lobe-dominated and core-dominated quasars, are the same class of object seen from different directions (Orr & Browne 1982). Extension of such a unified scheme to include high-luminosity (FRII) radio galaxies has been discussed by Scheuer (1987), Peacock (1987) and Barthel (1989). The question of whether low-luminosity (FRI) radio galaxies and BL Lac objects could be similarly unified has also received attention (Blandford & Rees 1978; Browne 1983; Antonucci & Ulvestad 1985; Urry & Padovani 1991). Some of the properties of core-dominated quasars seem difficult to reconcile with the Orr & Browne scheme (Boroson 1992; Heckman 1983; Schilizzi & de Bruyn 1983), but most studies of core-dominated quasars have used samples with ill-defined selection criteria which may have biased the results. In order to rectify this deficiency, we decided to observe a well-defined, complete sample of radio sources with the VLA.

In this paper (Paper I) we describe the selection criteria, VLA observations and data analysis of a sample of 89 core-dominated radio sources. The majority of these sources (70) are optically identified as quasars, and we leave a detailed comparison of their properties with the predictions of the unified schemes until Paper II. Here we discuss the properties of the BL Lacs in our sample, and the differences between the quasars defined as highly polarized quasars (HPQs) or optically violent variables (OVVs) and those known not to be HPQs/OVVs. When discussing BL Lacs, we confine ourselves to objects with featureless spectra or weak narrow lines only; we try to distinguish these objects from objects (OVVs/HPQs) with broad quasar-like lines that can on occasion be swamped by a powerful featureless con-

tinuum. Throughout this paper, unless stated otherwise, we use $H_0 = 50$ km s^{-1} Mpc^{-1} and $q_0 = 0$. We define the spectral index α by the relation $S \propto \nu^{-\alpha}$.

2 SAMPLE SELECTION

Previous work on core-dominated radio sources has shown that a significant number have extended radio emission on the arcsecond scale, but it is not clear what fraction of sources have extended emission, what the structure of this emission is and why we cannot detect it around all core-dominated sources. Are we limited by dynamic range, resolution or selection effects? In order to clarify these matters, we decided to map with the VLA a sample of core-dominated sources satisfying the following selection criteria.

(1) $|b| \geq 15°$.
(2) $S_{\rm core}(6\ {\rm cm}) \geq 1$ Jy.
(3) $\alpha(6\text{–}20\ {\rm cm}) \leq 0.5$.
(4) $\delta \geq 0°$.
(5) Optical identification: either a quasar or a BL Lac object. A BL Lac object was only included in our sample if it was found to be unresolved by Antonucci & Ulvestad (1985), if we thought we could improve on the Antonucci & Ulvestad map or if it was not in the Antonucci & Ulvestad sample but met our first four criteria.

The reasons for imposing these criteria are as follows. The first criterion was chosen because we wished to have sources with reliable optical identifications unaffected by Galactic obscuration. Since we wished to map the extended structure around core-dominated sources, we selected objects on the basis of core flux density alone, hence the second selection criterion. This also simplifies the statistical analysis. 5 GHz was chosen as our selection frequency because the Kühr et al. samples (1979, 1981), which contain many flat-spectrum core-dominated sources, were defined at this frequency, and these were the primary catalogues from which we selected sources. We used information on core strengths from Browne & Perley (1986) and unpublished VLA calibration observations to complement the Kühr et al. catalogues. Of the 89 sources that we eventually selected, 87 are contained in either the Kühr et al (1981) 1-Jy catalogue or the full Kühr et al. (1979) catalogue. One of the two sources not contained in either of these catalogues, but which is nevertheless included in our sample, is the superluminal quasar NRAO 140 (0333+321), which satisfies the general criteria to be included in the Kühr et al. surveys, namely (i) $S_{6\,\rm cm} \geq 1$ Jy, (ii) $|b| \geq 10°$. In the actual Kühr et al. catalogue, however, a few regions with $|b| \geq 10°$ are excluded, and NRAO 140 lies in one of these. The other source to be included in our sample, but also not contained in either of the Kühr et al. catalogues, is the BL Lac object 0754+100 which, because of core variability, had at our time of selection (1984) a core flux density in excess of 1 Jy. The third criterion was imposed because we wished to study flat-spectrum, core-dominated sources, and this criterion excludes the steep-spectrum, compact sources from our sample. The fourth criterion ensures that we get good instantaneous *uv* coverage with the VLA, a necessary requirement in that we wished to use the VLA in snapshot mode. The fifth and final requirement concerns the type of object. Since we hoped to test the predictions of the Orr & Browne (1982) unified scheme, which was designed to explain the differences between lobe-dominated and core-dominated quasars, we selected mainly quasars.

Relativistic beaming models have also been proposed to explain several of the properties of BL Lac objects. Blandford & Rees (1978) suggested that their unaligned counterparts are normal double radio sources, whereas Browne (1983) was more specific and argued that they are low-luminosity radio galaxies. Antonucci & Ulvestad (1985) discuss the high dynamic range maps that they and others have made of 37 BL Lac objects. They find extended emission associated with the compact cores to be common. Nevertheless, there remain several sources in which no such emission has been detected. We included in our sample all those BL Lacs that met our first four criteria and that either were not included in the Antonucci & Ulvestad compilation or were included but for which we felt that we could make significant improvements on the existing maps.

Of the 89 sources meeting our selection criteria, 70 are quasars and 19 are BL Lacs. Six more BL Lac objects (0048−097, 0521−365, 0829+046, 1147+245, 1652+398 and 1807+698) meet our first three selection criteria and have been observed by Antonucci & Ulvestad (1985). We include these when we discuss the properties of the BL Lacs in Section 6.1.

In Table 1, we list the objects in our sample, using the standard IAU nomenclature for the source name (epoch

Table 1. Radio sources in our sample.

Source Name	ID	redshift	$S_c(mJy)$	$S_e(mJy)$	LAS
0106+013	HPQ	2.107	3841.	421.0	4.5
0146+056	Q	2.345	865.	-	-
0149+218	Q	1.320	1089.	25.0	4.5
0202+149	HPQ	-	4419.	-	-
0202+319	nHPQ	1.466	965.	-	-
0229+131	nHPQ	2.065	1118.	212.0	4.7
0234+285	HPQ	1.207	2464.	107.0	5.6
0235+164	BL	0.940	972.	31.4	7.4
0256+075	BL	0.893	552.	39.0	5.2
0319+121	Q	2.670	1620.	15.9	12.9
0333+321	nHPQ	1.263	3326.	51.0	7.3
0400+258	Q	2.109	1382.	1.3	5.1
0422+004	BL	0.310	873.	-	-
0454+844	BL	-	533.	-	-
0457+024	Q	2.384	1626.	-	-
0615+820	Q	0.710	865.	-	-
0707+476	nHPQ	1.310	973.	94.0	3.4
0711+356	nHPQ	1.620	1543.	4.2	9.0
0735+178	BL	0.424	1915.	20.6	2.6
0738+313	nHPQ	0.630	2155.	65.0	30.0
0745+241	HPQ	0.410	719.	196.0	6.1
0748+126	nHPQ	0.889	1430.	27.0	8.6
0754+100	BL	0.670	2074.	6.7	6.1
0804+499	HPQ	1.433	643.	5.3	4.0
0814+425	BL	-	1571.	65.6	4.3
0820+225	BL	0.951	1606.	602.6	2.6
0823+033	BL	0.506	1325.	4.1	17.8
0828+493	BL	0.548	549.	-	-
0833+585	nHPQ	2.101	678.	30.0	9.6
0836+710	nHPQ	2.160	3743.	103.0	2.2
0839+187	nHPQ	0.259	1264.	7.0	23.5
0851+202	BL	0.306	1557.	-	-
0859+470	nHPQ	1.462	1645.	317.0	2.1
0906+015	HPQ	1.018	1002.	38.0	12.3
0917+624	nHPQ	1.440	1115.	6.4	5.0

Table 1 – *continued*

Source Name	ID	redshift	$S_c(mJy)$	$S_e(mJy)$	LAS
0923+392	nHPQ	0.698	2681.	655.0	3.8
0945+408	nHPQ	1.252	1228.	95.0	4.0
0953+254	nHPQ	0.712	483.	19.0	13.1
0954+556	HPQ	0.901	2568.	381.0	3.1
1040+123	nHPQ	1.029	1627.	1179.0	5.0
1055+018	HPQ	0.888	2642.	162.0	18.0
1055+201	nHPQ	1.110	768.	1826.0	21.4
1116+128	nHPQ	2.118	1888.	259.0	2.5
1117+146	Q	-	2280.	-	-
1128+385	Q	-	869.	5.4	16.4
1144+402	Q	1.010	1388.	2.7	10.8
1150+812	Q	1.250	1189.	24.5	5.1
1156+295	HPQ	0.729	1458.	244.0	3.0
1219+285	BL	0.102	1581.	-	-
1308+326	BL	0.996	1577.	67.9	11.5
1354+195	nHPQ	0.720	1309.	855.0	28.4
1404+286	nHPQ	0.077	991.	-	-
1418+546	BL	0.152	1189.	22.0	36.8
1442+101	Q	3.530	2438.	-	-
1502+106	HPQ	1.833	2198.	23.0	7.0
1538+149	BL	0.605	1330.	202.0	2.8
1546+027	HPQ	0.412	1147.	18.8	31.1
1548+056	HPQ	1.422	2560.	-	-
1606+106	nHPQ	-	1347.	26.5	6.5
1611+343	nHPQ	1.401	2833.	20.6	10.7
1624+416	Q	2.550	1607.	-	-
1633+382	nHPQ	1.814	2170.	32.0	7.0
1637+574	nHPQ	0.750	1188.	150.0	5.3
1641+399	HPQ	0.594	8500.	1010.0	2.8
1642+690	HPQ	0.751	999.	330.0	3.6
1655+077	HPQ	0.621	1165.	211.0	4.0
1656+053	HPQ	0.879	1301.	96.0	2.4
1656+477	Q	1.622	732.	-	-
1749+096	BL	0.320	903.	-	-
1803+784	HPQ	0.684	1557.	68.0	45.0
1823+568	BL	0.644	858.	452.0	10.4
1828+487	nHPQ	0.691	4500.	7781.0	6.0
1928+738	nHPQ	0.302	2939.	243.0	18.0
2007+777	BL	0.342	823.	28.9	21.4
2121+053	HPQ	1.878	1084.	4.8	2.8
2134+004	nHPQ	1.936	4818.	6.6	3.1
2136+141	nHPQ	2.427	1140.	-	-
2144+092	Q	1.113	698.	82.0	2.3
2145+067	nHPQ	0.990	2656.	16.0	2.6
2201+315	nHPQ	0.298	1400.	384.0	37.0
2223+210	nHPQ	1.959	1766.	47.0	4.9
2230+114	HPQ	1.037	6468.	286.0	2.8
2234+282	HPQ	0.795	1118.	3.4	4.9
2247+140	nHPQ	0.237	1860.	-	-
2251+158	HPQ	0.859	12190.	755.0	5.4
2253+417	Q	1.476	1342.	-	-
2254+074	BL	0.190	525.	-	-
2328+107	nHPQ	1.489	1065.	25.0	21.1
2344+092	nHPQ	0.673	1801.	26.0	4.1

Notes. This table contains information on the 89 sources in our sample. Columns are as follows. (1) Source name. (2) ID: optical identification, where HPQ = HPQ quasar, nHPQ = non-HPQ quasar, Q = quasar and BL = BL Lac. (3) Redshift. (4) S_c (mJy), core flux density in mJy. (5) S_e (mJy), extended flux density in mJy. (6) LAS, largest angular size in arcsec.

1950.0), together with their redshifts, if known. Sources are generally classified as BL Lacs if they are listed in the BL Lac catalogue of Burbidge & Hewitt (1987), if they are confirmed or probable BL Lac objects in table 2 of the Véron-Cetty & Véron catalogue (1991), or if they appear in the Stickel et al. (1991) complete sample of BL Lacs. Other optical identifications are given in the Kühr et al. (1979) catalogue, with the exception of NRAO 140 and 1624+416. As stated above, NRAO 140 is not in the Kühr et al. (1979) catalogue, but is a well-known quasar (Kristian & Sandage 1970). 1624+416 is reported to be a quasar with $z = 2.55$ by Pearson & Readhead (1988). Most of the redshifts for the quasars are taken from the Véron-Cetty & Véron catalogue (1991), with the exceptions of those for 0319+121, 0745+241 and 0917+624, which were kindly provided by Dr H. Kühr (private communication), and 0707+476 (Browne & Perley 1986). The BL Lac redshifts are those given in the Burbidge & Hewitt catalogue or are taken from Stickel et al. (1991), with the exceptions of 0422+004, 0754+100, 0829+046, 1057+100 and 1215+303, whose redshifts were obtained from a search of the NASA/IPAC extragalactic data base (NED) in 1992 March.

3 OBSERVING REQUIREMENTS

The VLA was chosen because it is the only instrument capable of providing maps with high dynamic range and a resolution of 1 arcsec for a sample of $\simeq 100$ sources without the need for a prohibitive amount of observing time. Our requirements were as follows. First, we wished to detect low-level extended emission (if present). This implied that we needed high dynamic range ($\geq 1000{:}1$ peak:rms). Secondly, we needed sufficient resolution to study the structure of the extended emission. These requirements were met by the following observing strategy:

(1) observe in the *L* band (20 cm) to maximize the ability to detect steep-spectrum extended emission;

(2) observe at two separated frequencies within the band to achieve maximum *uv* coverage;

(3) observe in both the A and B configurations and combine data afterwards to increase the ability to detect extended emission while still maintaining 1-arcsec resolution;

(4) observe each source at five different Hour Angles for approximately 2 min each to improve *uv* coverage;

(5) observe at maximum available bandwidth to achieve maximum sensitivity.

The A-array observations took place on 1984 December 24 and the B-array observations on 1985 April 27, at the frequencies 1465 MHz (bandwidth = 50 MHz) and 1640 MHz (bandwidth = 25 MHz). It was not possible to use the full 50-MHz bandwidth available at 1640 MHz because of interference from the *GLONASS* satellites.

4 DATA ANALYSIS

The initial calibration of our VLA data was performed on the Dec-10 computer at the VLA, and most of the subsequent analysis was also done at the VLA using the Astronomical Image Processing Software (AIPS) package. We had to develop a novel technique in order to make high dynamic

range maps from our data observed at two epochs, at two frequencies, and with two different arrays. The procedure was as follows.

Having calibrated the data, we wanted to make maps with high dynamic range, but we could not simply add all the data together, for three main reasons:

(1) core-variability – the A- and B-array observations were taken four months apart, during which several of the cores varied by as much as 30 per cent;

(2) spectral-index effects – we observed at two separated frequencies in the L band and, because the extended emission has a different spectral index from the core, the relative flux densities of the components are different at the two frequencies;

(3) misalignment of phase centres – we observed at several epochs and frequencies, so there is no guarantee that the phase centres for each observation are the same.

In order to understand how these effects change the observed visibility compared to the visibility obtained at a reference frequency and epoch, we consider the following simple representation of the brightness distribution of a core-dominated radio source. Let the brightness distribution at an epoch t and observing frequency ν, $B(\nu, t, x, y)$, be represented by

$$B(\nu, t, x, y) = C(\nu, t)\,\delta(x, y) + E(\nu, x, y).$$

Here we assume that the core (C) is at the phase centre and the extended emission (E) is not time variable. If we further assume that the extended emission has a constant spectral index, α_e, then it follows from the van-Cittert Zernicke theorem that the visibility measured at a given frequency and epoch for particular values of u and v, $V(\nu, t, u, v)$, is related to the visibility at a reference time and frequency, $V(\nu_0, t_0, u, v)$, as follows:

$$V(\nu_0, t_0, u, v) = (\nu/\nu_0)^{\alpha_e}[V(\nu, t, u, v) - C(\nu, t) + (\nu_0/\nu)^{\alpha_e} C(\nu_0, t_0)].$$

Thus, if we are to combine the visibilities at different epochs and frequencies into a single data set, we have to adjust the visibilities to make them consistent with one another. This can be accomplished in two steps. First, we can adjust the core so that it has an overall spectral index α_e. That is, we change the core $C(\nu, t)$ by an amount $\Delta C(\nu, t) = (\nu_0/\nu)^{\alpha_e} C(\nu_0, t_0) - C(\nu, t)$. With this change, $V(\nu_0, t_0, u, v) = (\nu/\nu_0)^{\alpha} V(\nu, t, u, v)$. Secondly, we multiply the corrected visibility at (ν, t) by $(\nu/\nu_0)^{\alpha_e}$. For our observations, however, we observed at two frequencies at two epochs and so had to proceed in a slightly more complicated fashion as we now describe.

Experience with the VLA has shown that, in circumstances where the dynamic range is not already limited by thermal noise, baseline-based error correction is needed to achieve dynamic ranges greater than a few thousand to one (Perley 1989). We therefore applied baseline-based corrections to our visibility data by working out the closure offsets for one strong point source 2134+004 and applying these corrections to the rest of our data. After applying these corrections, the four individual data sets were mapped and self-calibrated. Then we combined the data from the different epochs (A and B arrays) at a given frequency, having first adjusted the A-array core flux density so that it equalled the B-array core flux density. The combined upper-frequency (ν_2) data set was then mapped, and the resulting clean components were used as a model in the self-calibration of the combined lower frequency (ν_1) data set whose core had been adjusted to have a spectral index of 0.7 with respect to the combined upper frequency core flux density. In this self-calibration the sum of gains of the antennas was allowed to vary, which has the result of multiplying the lower frequency data set by an amount $(\nu_1/\nu_2)^{\alpha_e}$. The combined frequency and epoch data set was then mapped and self-calibrated several times to produce the final image. For several sources the dynamic range that could be obtained was limited by nearby confusing objects. The effects of such confusion were removed by mapping a large field around the source to identify the position of the confusing sources. Having found their positions, this large field could be remapped by performing a multi-field clean, and the resulting clean components could then be subtracted from the combined data set to leave a set of visibilities from which the effects of confusing sources had been largely removed. From this data set we were then able to produce a high dynamic range image of the main source. This procedure worked successfully and produced much higher fidelity images than would have been obtained by adding together our four initial data sets without any corrections. The typical dynamic range of our images is 5000–10 000:1, where dynamic range is defined as peak to rms noise level and the typical rms noise level is 0.1–0.4 mJy beam^{-1}.

5 MAPS

The maps for the 68 out of 89 sources for which we detected extended emission are shown in Fig. 1. Table 2 lists, for each map, the peak flux density in Jy beam^{-1}, the major axis of the CLEAN restoring beam in arcsec, the minor axis of the CLEAN restoring beam in arcsec, the position angle (PA) of the major axis of the CLEAN restoring beam in degrees, and the parameters CLEV and MLEV which determine the contour levels. The contour levels used for each map are CLEV * (-4, -3, -2, -1, 1, 2, 3, 4, 8, 16, 32,...,MLEV) mJy beam^{-1}, where the higher levels increase in powers of two to a maximum of MLEV.

6 DISCUSSION

We leave a discussion of the properties of the quasars and how they compare with the predictions of the relativistic unified schemes until Paper II. Here we consider the BL Lac objects and the differences in properties between those quasars classified as HPQs (high-polarization quasars) and those classified as non-HPQs. In Table 1 there are 70 quasars and 19 BL Lac objects. Of the 70 quasars, we can find references in the literature to 21 being HPQs (quasars having optical polarizations in excess of 3 per cent at one or more epochs) and to 34 being non-HPQs (quasars having measured optical polarization never in excess of 3 per cent). We also list the core flux densities. If we detected extended emission around a source, then we list in Table 1 the extended flux density and largest angular size, which is measured from the core to the peak in the extended radio structure. We adopt this, rather than the usual 'two-sided' definition because, for some objects, emission is detected on only one side of the core. Angular sizes could thus be

measured for all the objects in our sample with detected emission.

We have a problem with measuring angular sizes when we come to use the observations of BL Lac objects listed by Antonucci & Ulvestad (1985). This is that many of their maps are of lower resolution than our A+B configuration maps, and the former tend to show diffuse halo emission for which it is very difficult to define a consistent angular size with our, or for that matter any other, definition. Rather than run the risk of not comparing like with like, for example when we

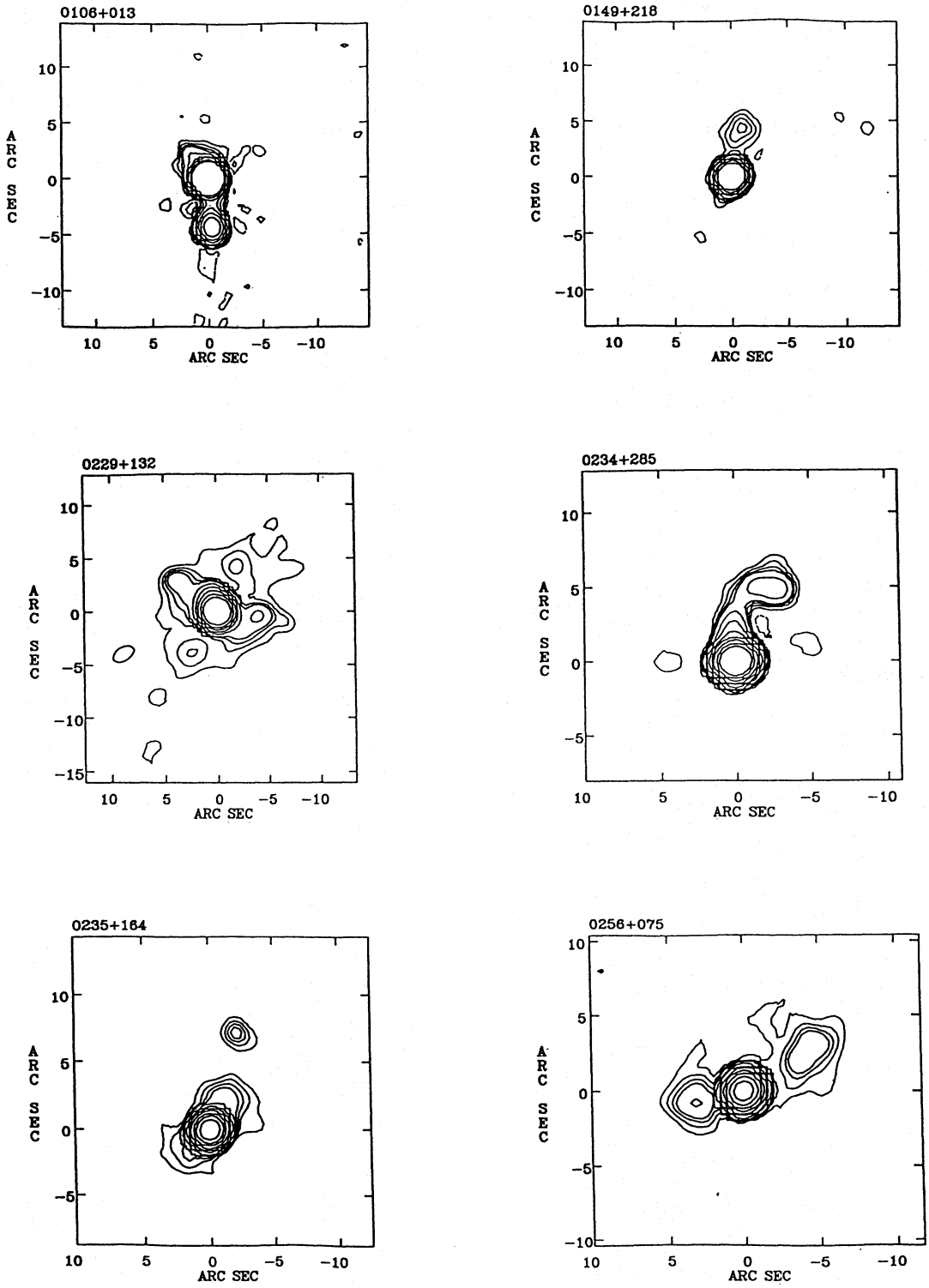

Figure 1. Maps of the 68 sources in our sample with detected extended radio emission. Contour levels used are CLEV*(−4, −3, −2, −1, 1, 2, 3, 4, 8, 16, 32,...,MLEV) mJy beam^{-1}, where CLEV, MLEV and the restoring beam are listed in Table 2.

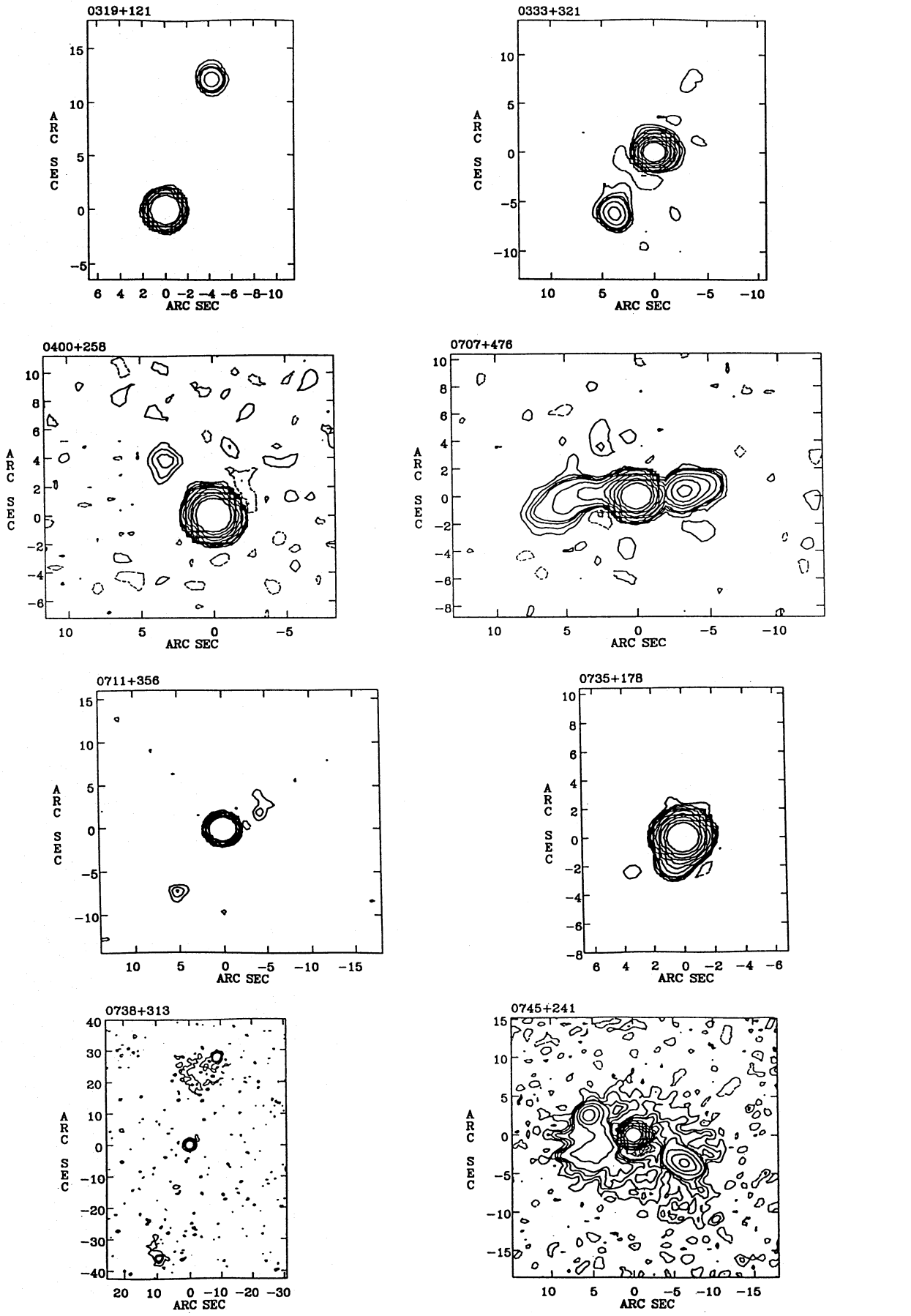

Figure 1 – *continued*

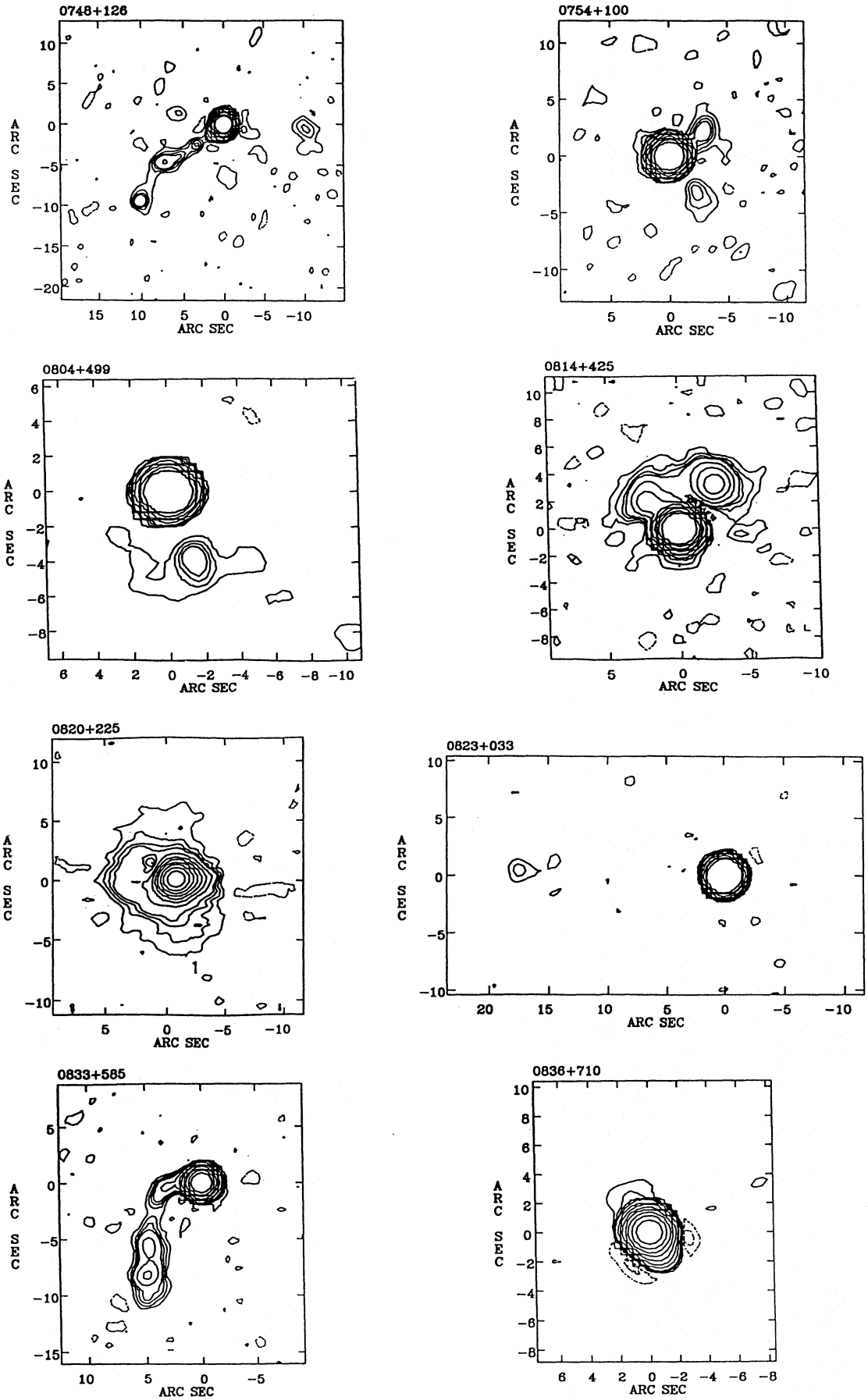

Figure 1 – *continued*

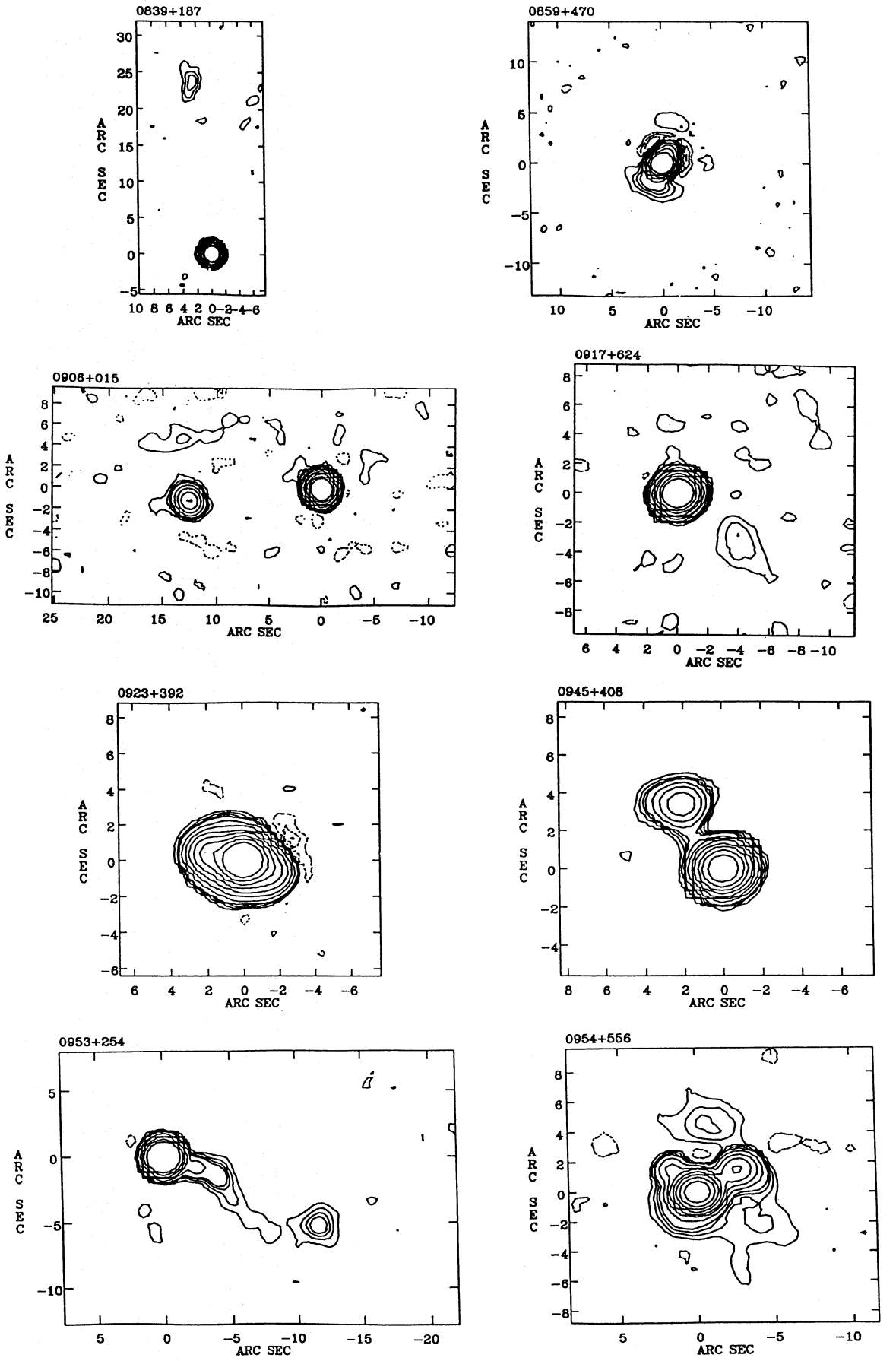

Figure 1 – *continued*

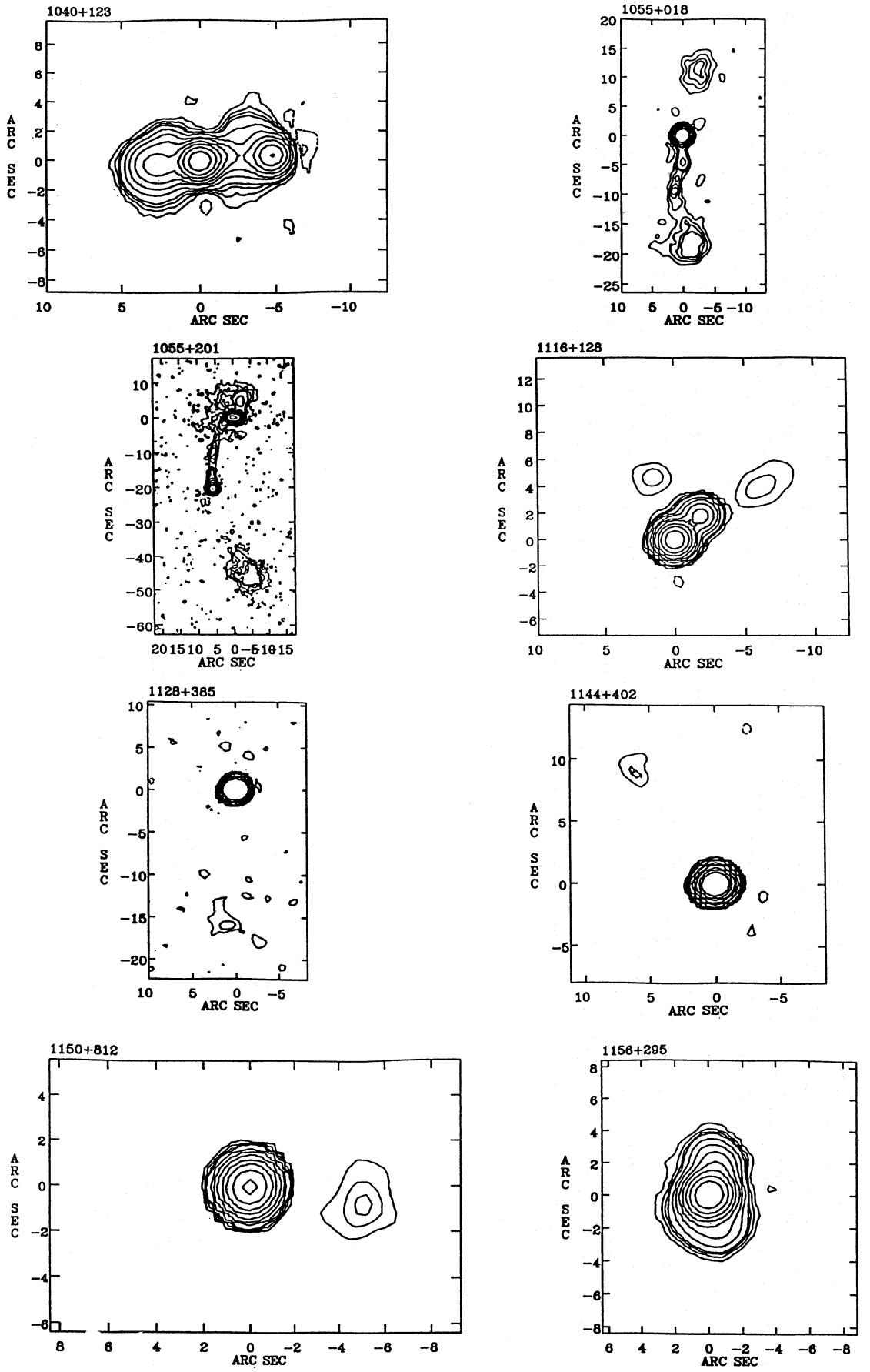

Figure 1 – *continued*

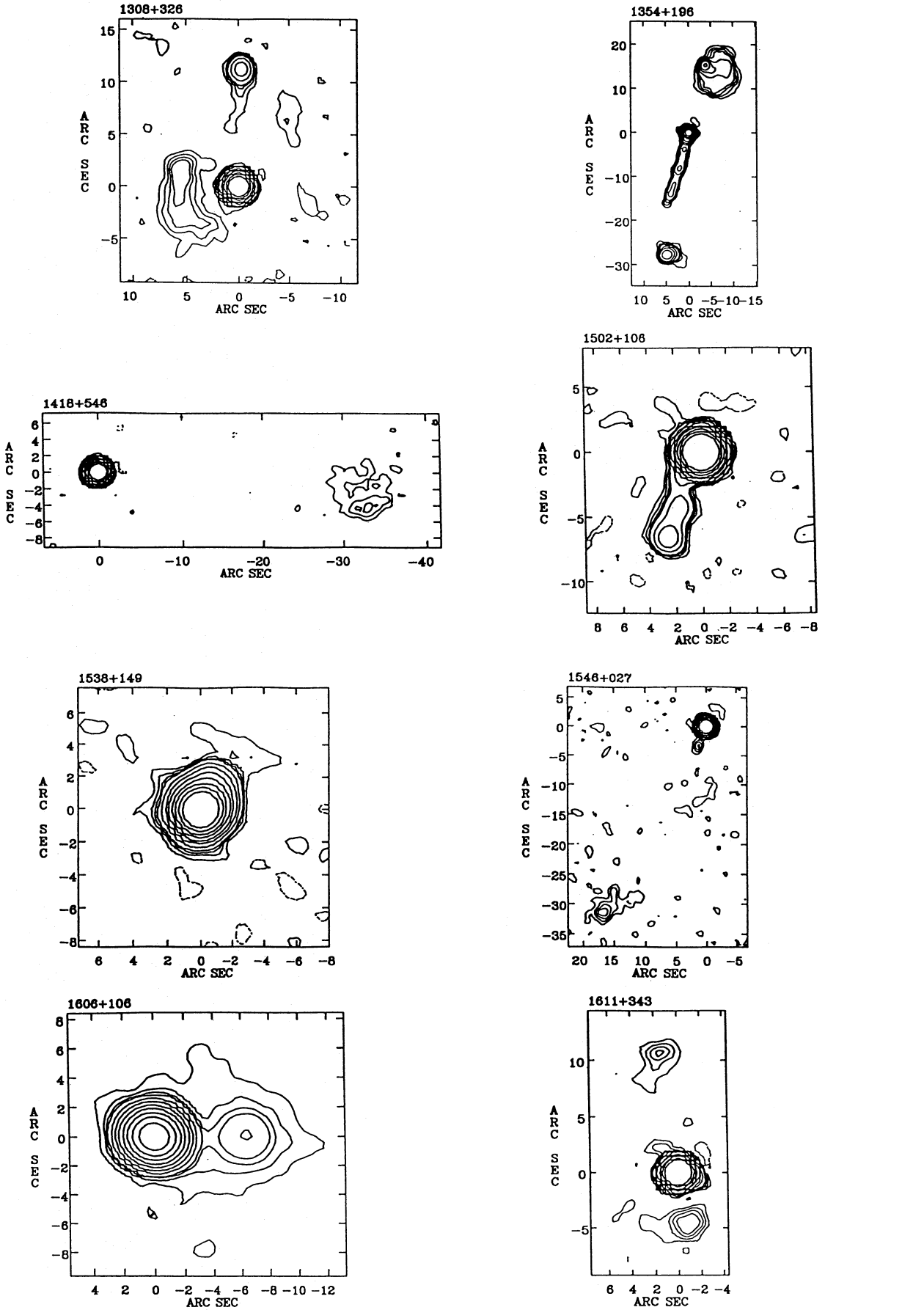

Figure 1 – *continued*

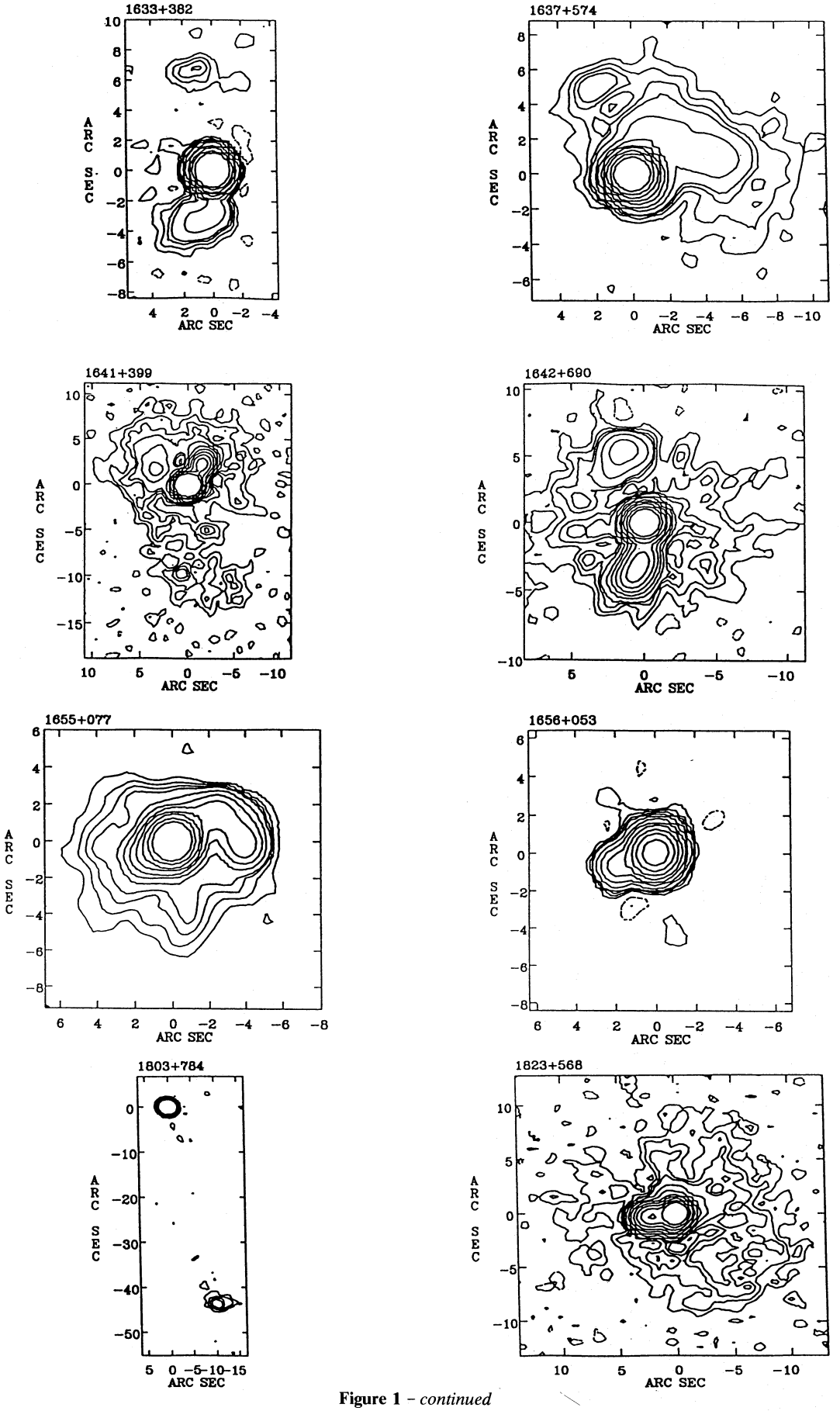

Figure 1 – *continued*

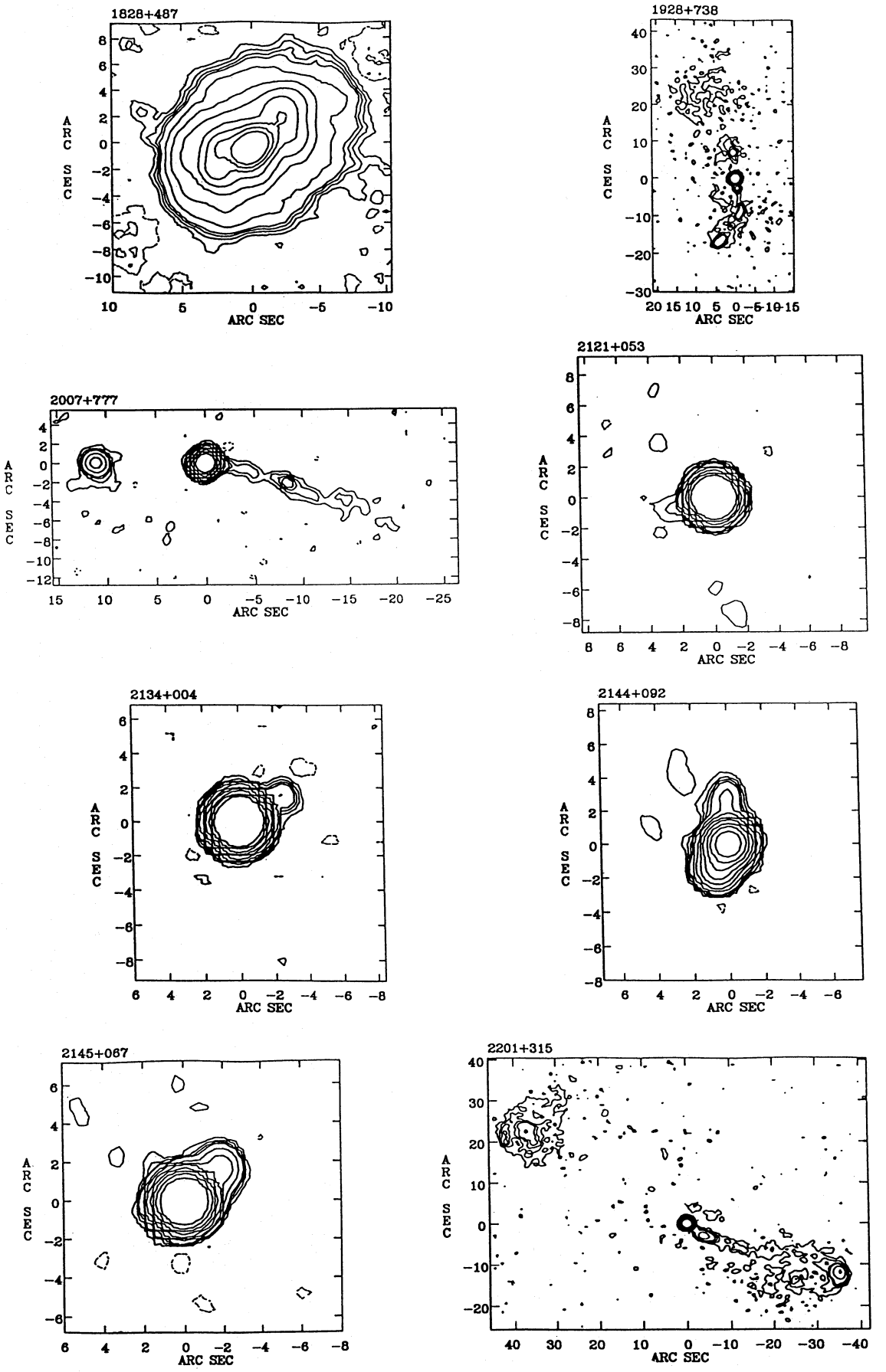

Figure 1 – *continued*

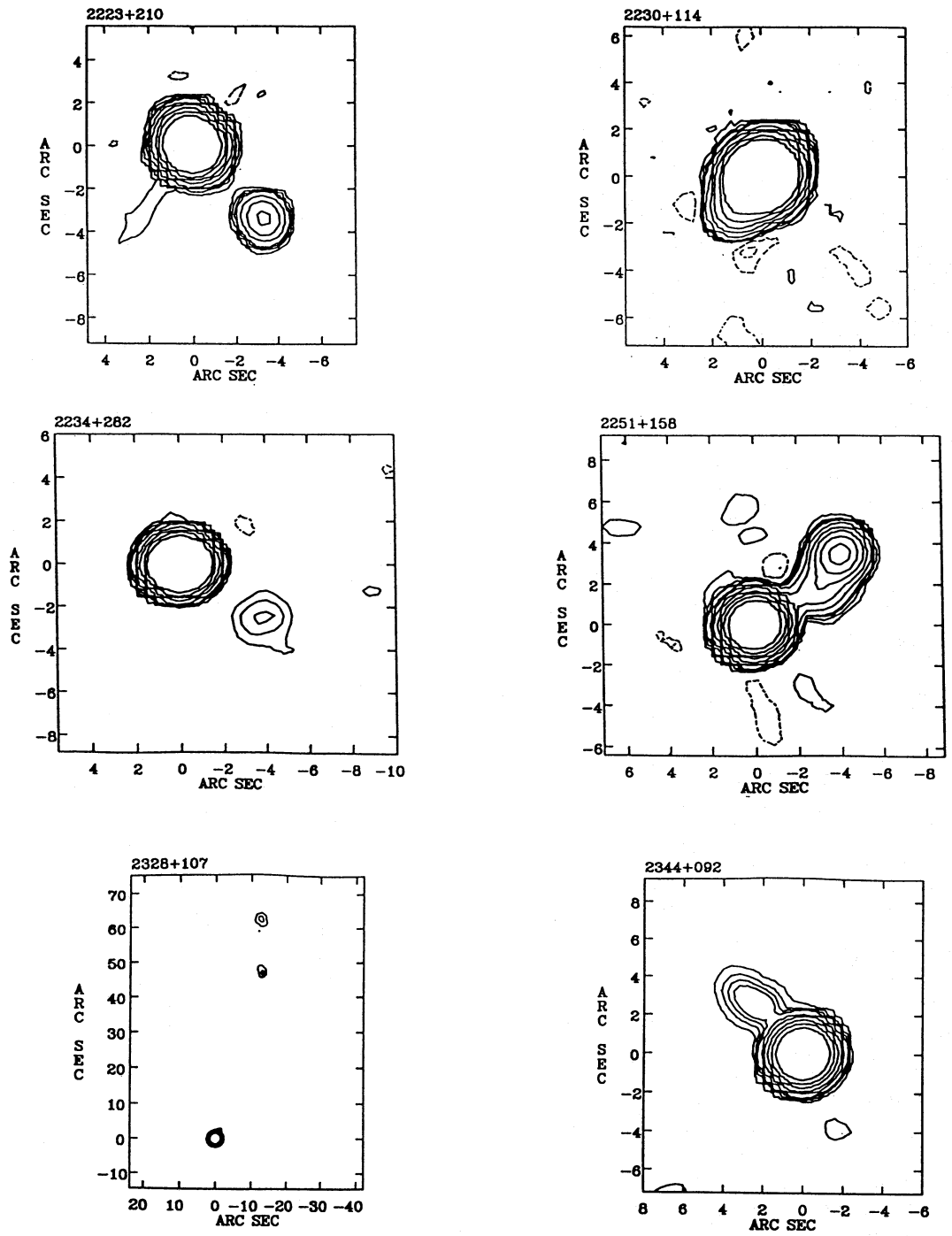

Figure 1 – *continued*

look for differences between the sizes of BL Lacs and quasars, we only quote sizes for sources that we have observed, or for those with maps in the literature of the same resolution as ours. In Table 4, if a BL Lac has a R_o value but no angular size, then it is a BL Lac in the Antonucci & Ulvestad (1985) sample for which we could not find a map of comparable resolution to ours.

Derived properties for the quasars in our sample are given in Table 3, and for the BL Lacs in Table 4. One of the derived properties to which we pay particular attention is the ratio of core to extended flux density, which is called the R parameter (Orr & Browne 1982). It is useful to distinguish between two R parameters, R_o and R_c. R_o is simply the ratio of core to extended flux density at the observing frequency, whereas R_c is the ratio of core to extended luminosity at an emitted frequency equal to the observing frequency. Adopting the assumptions of Orr & Browne (1982), it is found that

$$R_c = R_o/(1+z), \qquad (1)$$

Table 2. Map parameters for the 68 sources in our sample with extended radio emission.

Source	Peak Flux Jy/beam	Major axis "	Minor axis "	PA °	CLEV	MLEV
0106+013	3.84	1.39	1.30	21.2	1.10	128
0149+218	1.09	1.31	1.27	-67.9	0.90	128
0229+132	1.12	1.69	1.59	83.6	1.60	128
0234+285	2.46	1.36	1.25	-86.0	0.99	512
0235+164	0.97	1.35	1.31	-69.5	0.78	512
0256+075	0.55	1.32	1.29	-37.1	0.55	512
0319+121	1.62	1.32	1.29	30.6	0.81	128
0333+321	3.31	1.38	1.27	85.4	1.32	512
0400+258	1.38	1.36	1.25	76.9	0.28	512
0707+476	0.97	1.36	1.20	-86.7	0.39	512
0711+356	1.54	1.37	1.22	87.8	0.48	128
0735+178	1.92	1.37	1.30	85.2	0.77	512
0738+313	2.16	1.35	1.24	-87.6	0.43	512
0745+241	0.72	1.33	1.27	88.0	0.36	512
0748+126	1.43	1.33	1.32	-83.4	0.57	512
0754+100	2.07	1.35	1.34	-53.3	0.41	512
0804+499	0.64	1.35	1.20	79.7	0.36	128
0814+425	1.57	1.33	1.20	78.8	0.31	512
0820+225	1.61	1.37	1.25	85.6	1.60	512
0823+033	1.33	1.34	1.33	12.4	0.45	128
0833+585	0.68	1.35	1.22	-88.9	0.34	512
0836+710	3.90	1.55	1.44	76.4	3.12	512
0839+187	1.26	1.38	1.33	60.8	0.51	512
0859+470	1.84	1.46	1.26	-89.2	2.95	512
0906+015	1.00	1.36	1.29	30.9	0.40	512
0917+624	1.11	1.34	1.24	-79.1	0.45	512
0923+392	2.68	1.35	1.20	87.2	1.07	512
0945+408	1.23	1.38	1.22	-88.8	0.98	512
0953+254	0.48	1.33	1.26	87.7	0.39	128
0954+556	2.58	1.47	1.23	-89.3	2.06	512
1040+123	1.63	1.37	1.31	-81.9	1.63	512
1055+018	2.64	1.36	1.31	-30.5	1.06	512
1055+201	0.77	1.65	1.50	-84.7	1.23	512
1116+128	1.89	1.41	1.39	-30.8	1.89	512
1128+385	0.87	1.35	1.20	86.5	0.35	128
1144+402	1.39	1.35	1.23	-85.4	0.55	512
1150+812	1.19	1.31	1.30	-32.5	1.88	512
1156+295	1.46	1.46	1.43	-55.3	1.19	512
1308+326	1.58	1.32	1.22	74.7	0.63	512
1354+196	1.31	1.39	1.31	-87.8	1.31	512
1418+546	1.19	1.30	1.22	-89.5	0.47	512
1502+106	2.20	1.51	1.48	48.6	0.44	512
1538+149	1.33	1.40	1.35	66.9	0.53	512
1546+027	1.15	1.41	1.36	23.8	0.46	512
1606+106	1.35	2.03	1.83	67.5	1.35	512
1611+343	2.83	1.30	1.21	81.2	0.57	512
1633+382	2.17	1.30	1.21	80.6	0.43	512
1637+574	1.19	1.30	1.22	-86.7	0.47	512
1641+399	8.50	1.29	1.19	82.2	0.85	512
1642+690	1.00	1.31	1.28	-58.0	0.40	512
1655+077	1.16	1.35	1.34	-29.3	0.47	512
1656+053	1.30	1.37	1.31	-15.8	1.30	512
1803+784	1.88	1.70	1.39	77.0	0.44	128
1823+568	0.86	1.38	1.21	-86.8	0.34	512
1828+487	4.50	1.32	1.20	-86.4	1.80	512
1928+738	2.94	1.27	1.26	-14.8	0.59	512
2007+776	0.82	1.27	1.24	-35.7	0.33	512
2121+053	1.08	1.42	1.36	29.6	0.60	128
2134+004	4.82	1.40	1.32	3.3	0.48	512
2144+092	0.70	1.33	1.29	-0.7	0.56	512
2145+067	2.66	1.33	1.31	1.2	0.53	512
2201+315	1.40	1.35	1.22	78.4	0.56	512
2223+210	1.77	1.35	1.28	84.1	1.10	128
2230+114	6.47	1.34	1.32	-16.6	1.60	128
2234+282	1.12	1.38	1.23	88.6	0.43	128
2251+158	12.19	1.34	1.31	-65.6	2.60	512
2328+107	1.06	1.56	1.55	-22.1	0.90	128
2344+092	1.80	1.54	1.54	40.5	1.90	128

where z is the redshift of the object. According to the simple beaming models, the ratio R_c depends on the angle to the line of sight of the motion in the object's core which is assumed to define the source axis. Thus objects with low R_c have large angles to the line of sight, and those with high R_c have small angles to the line of sight.

6.1 BL Lac objects

We combine our sample of 19 BL Lac objects with those studied by Antonucci & Ulvestad (1985) in two ways. First, we produced a well-defined sample of 25 BL Lac objects, which we call the restricted sample, satisfying our first three criteria, namely

$$|b| \geq 15°, \qquad S_{\rm core}(6\ {\rm cm}) \geq 1\ {\rm Jy}, \qquad \alpha(6\text{–}20\ {\rm cm}) \leq 0.5.$$

Secondly, we merged all the BL Lacs in our two samples to form a combined sample of 45 BL Lacs. Table 4 lists these sources. For sources with $\delta \geq 0°$, we have compared our restricted sample of BL Lac objects with the Kühr & Schmidt (1990) complete sample of BL Lac objects that have 5-GHz flux densities > 1 Jy and are in the Kühr et al. survey (1981). In our sample there are four BL Lac objects not in the Kühr & Schmidt sample (0422+004, 0754+100, 0829+046 and 1219+285). All four may have been excluded because of core variability and different epochs of selection. Seven BL Lac objects in the Kühr & Schmidt sample are not in ours (0119+11, 0716+71, 0954+65, 1732+38, 1749+70, 2150+17 and 2200+42). Again, their absence can be understood in terms of core variability, the fact that we selected sources on the basis of their core flux density rather than, as Kühr & Schmidt did, on the basis of total flux density, and different galactic latitude selection criteria.

One question that has been tackled by many authors is where BL Lac objects fit into the relativistic beaming scenarios. Along with OVV/HPQ quasars they exhibit many properties that can be explained by relativistic beaming, namely being highly time-variable at all wavelengths, having large swings of polarization position angle, showing a deficit of inverse Compton X-rays compared to that expected for a stationary emitter, and having weak or no emission lines, presumably indicative of a highly beamed optical continuum, and (in the case of a few BL Lacs) modest superluminal motion (Cohen 1989). So extreme are the properties of

Table 3. Derived parameters for the 70 quasars in our sample.

Source	ID	Log(R_o)	Log(R_c)	LLS	Log(L_{ext})
0106+013	HPQ	0.960	0.468	58.7	28.53
0146+056	Q	-	-	-	-
0149+218	Q	1.639	1.274	53.3	26.71
0202+149	HPQ	-	-	-	-
0202+319	nHPQ	-	-	-	-
0229+131	nHPQ	0.722	0.236	61.1	28.20
0234+285	HPQ	1.362	1.018	64.8	27.23
0319+121	Q	2.008	1.443	173.8	27.42
0333+321	nHPQ	1.814	1.460	85.5	26.97
0400+258	Q	3.027	2.534	66.5	26.02
0457+024	Q	-	-	-	-
0615+820	Q	-	-	-	-
0707+476	nHPQ	1.015	0.651	40.2	27.28
0711+356	nHPQ	2.565	2.147	111.9	26.19
0738+313	nHPQ	1.521	1.308	272.2	26.28
0745+241	HPQ	0.564	0.415	44.1	26.31
0748+126	nHPQ	1.724	1.448	90.1	26.28
0804+499	HPQ	2.084	1.698	48.4	26.14
0833+585	nHPQ	1.354	0.863	125.2	27.38
0836+710	nHPQ	1.560	1.061	28.8	27.95
0839+187	nHPQ	2.257	2.157	126.2	24.41
0859+470	nHPQ	0.715	0.324	25.5	27.94
0906+015	HPQ	1.421	1.116	135.0	26.58
0917+624	nHPQ	2.241	1.854	60.5	26.22
0923+392	nHPQ	0.612	0.382	36.1	27.39
0945+408	nHPQ	1.111	0.759	46.7	27.23
0953+254	nHPQ	1.405	1.172	125.6	25.88
0954+556	HPQ	0.829	0.550	32.6	27.44
1040+123	nHPQ	0.140	-0.167	55.1	28.09
1055+018	HPQ	1.212	0.936	188.4	27.06
1055+201	nHPQ	-0.376	-0.700	241.4	28.37
1116+128	nHPQ	0.863	0.369	32.6	28.32
1117+146	Q	-	-	-	-
1128+385	Q	2.207	-	-	-
1144+402	Q	2.711	2.408	118.2	25.43
1150+812	Q	1.686	1.334	59.5	26.63
1156+295	HPQ	0.776	0.539	29.0	27.01
1354+195	nHPQ	0.185	-0.051	273.5	27.54
1404+286	nHPQ	-	-	-	-
1442+101	Q	-	-	-	-
1502+106	HPQ	1.980	1.528	89.2	27.08
1546+027	HPQ	1.785	1.636	225.5	25.30
1548+056	HPQ	-	-	-	-
1606+106	nHPQ	1.706	-	-	-
1611+343	nHPQ	2.138	1.758	128.7	26.70
1624+416	Q	-	-	-	-
1633+382	nHPQ	1.831	1.382	89.0	27.21
1637+574	nHPQ	0.899	0.656	51.9	26.83
1641+399	HPQ	0.925	0.723	24.7	27.41
1642+690	HPQ	0.481	0.238	35.3	27.18
1655+077	HPQ	0.742	0.532	36.1	26.78
1656+053	HPQ	1.132	0.858	25.0	26.82
1656+477	Q	-	-	-	-
1803+784	HPQ	1.360	1.133	423.9	26.39
1828+487	nHPQ	-0.238	-0.466	56.8	28.46
1928+738	nHPQ	1.083	0.968	107.4	26.10
2121+053	HPQ	2.354	1.895	35.8	26.43
2134+004	nHPQ	2.863	2.396	39.9	26.61
2136+141	nHPQ	-	-	-	-
2144+092	Q	0.930	0.605	26.0	27.02
2145+067	nHPQ	2.220	1.921	28.3	26.17
2201+315	nHPQ	0.562	0.449	218.8	26.28
2223+210	nHPQ	1.575	1.104	63.2	27.48
2230+114	HPQ	1.354	1.045	30.9	27.48
2234+282	HPQ	2.517	2.263	49.2	25.25
2247+140	nHPQ	-	-	-	-
2251+158	HPQ	1.208	0.939	55.8	27.69
2253+417	Q	-	-	-	-
2328+107	nHPQ	1.629	1.233	257.4	26.86
2344+092	nHPQ	1.841	1.617	38.3	25.95

Notes. This table contains derived information on the 70 quasars in our sample. Columns are as follows.
(1) Source name.
(2) Source ID: HPQ = high-polarization quasar; nHPQ = low-polarization quasar; Q = quasars for which we found no polarization information in the literature.
(3) Log(R_0) at 1.64 GHz, where R_0 is the ratio of core to extended flux density.
(4) Log(R_c) at 1.64 GHz emitted, where R_c is ratio of core to extended luminosity at an emitted frequency equal to the observing frequency, assuming that the core is flat-spectrum ($\alpha = 0$) and the extended emission is steep-spectrum ($\alpha = 1$), i.e. $R_c = R_0/(1+z)$.
(5) Largest linear size (LLS) in kpc.
(6) Log(L_{ext}), where L_{ext} = extended radio luminosity in W Hz^{-1} at 1.64 GHz.

BL Lacs that several authors have proposed that they are objects viewed along the axis of a relativistic jet (Blandford & Rees 1978). If this is the case, the question naturally arises as to what are the unbeamed counterparts to BL Lac objects. Blandford & Königl (1979), in their discussion of the optical observations of compact radio sources, suggested that the sequence radio-quiet quasars, radio-loud quasars, OVV quasars and BL Lac objects corresponds to intrinsically similar strong sources whose jets are viewed at progressively decreasing angles to their axes.

Though our view is that the majority of objects classified as BL Lacs are not directly related to quasars, but rather to low-luminosity (FRI) radio galaxies (Browne 1983; Peacock 1987; Urry & Padovani 1991), this is not universally accepted (Cohen 1989; Ostriker & Vietri 1990). The present data enable us to check whether or not BL Lac objects have properties consistent with them being the most beamed quasars. If this were so, we would expect BL Lac objects to have higher R values than quasars in our sample, but similar redshift and extended radio luminosity distributions. In Figs 2 and 3 we show the R_o distributions for the quasars in our sample, and for both the restricted and combined BL Lac samples. We test whether or not the distributions are statistically distinguishable using the Kolmogorov–Smirnov statistic, which we also plot in the right-hand panel of each figure. There is a tendency for the BL Lac objects to have *lower* R_o values than the quasars rather than higher, but the difference is not statistically significant at the 95 per cent confidence level. The results therefore offer no support for the view that BL Lacs are quasars with more highly beamed cores.

Table 4. Table of 45 BL Lacs that are contained in our sample and the Antonucci & Ulvestad (1985) sample.

Name	ID	Z	Log(R_o)	Log(R_c)	LAS(")	LLS	Log(L_{ext})
0048-097	1	-	1.010	-	-	-	-
0109+224	2	-	1.660	-	-	-	-
0215+015	2	1.715	0.860	0.426	3.9	49.0	27.51
0219+428	2	0.444	-0.070	-0.230	-	-	27.08
0235+164	1	0.940	1.491	1.203	7.4	79.1	26.41
0256+075	1	0.893	1.151	0.874	5.2	54.5	26.44
0300+470	2	-	1.570	-	9.8	-	-
0422+004	1	0.310	-	-	-	-	-
0454+844	1	-	-	-	-	-	-
0521-365	1	0.061	-0.450	-0.476	-	-	26.17
0548-322	2	0.069	-0.390	-0.419	-	-	24.63
0735+178	1	0.424	1.968	1.815	2.6	19.2	25.37
0754+100	1	0.670	2.491	2.268	6.1	56.9	25.36
0808+019	2	-	1.590	-	5.0	-	-
0814+425	1	-	1.379	-	4.3	-	-
0818-128	2	-	0.270	-	-	-	-
0820+225	1	0.951	0.426	0.135	2.6	27.9	27.70
0823+033	1	0.506	2.509	2.332	17.8	144.8	24.85
0828+493	1	0.548	-	-	-	-	-
0829+046	1	0.250	1.010	0.913	-	-	25.33
0851+202	1	0.306	-	-	-	-	-
0912+297	2	-	0.340	-	-	-	-
1057+100	2	0.186	0.740	0.666	-	-	24.97
1101+384	2	0.031	0.500	0.487	-	-	23.84
1133+704	2	0.046	-0.220	-0.240	-	-	24.31
1147+245	1	-	1.470	-	-	-	-
1215+303	2	0.237	0.320	0.228	-	-	25.71
1219+285	1	0.102	-	-	-	-	-
1308+326	1	0.996	1.366	1.066	11.5	125.3	26.81
1400+162	2	0.245	-0.330	-0.425	3.1	16.0	26.21
1418+546	1	0.152	1.733	1.671	36.8	132.0	24.40
1514+197	2	-	2.220	-	10.5	-	-
1514-241	2	0.049	1.950	1.929	7.1	9.4	23.49
1538+149	1	0.605	0.819	0.613	2.8	24.9	26.73
1652+398	1	0.034	1.350	1.335	-	-	23.49
1717+178	2	-	1.820	-	8.6	-	-
1727+502	2	0.055	0.590	0.567	-	-	23.79
1749+096	1	0.320	-	-	-	-	-
1807+698	1	0.051	0.170	0.148	24.8	34.2	25.02
1823+568	1	0.644	0.278	0.062	10.4	95.3	27.15
2007+777	1	0.342	1.455	1.327	21.4	138.5	25.30
2032+107	2	0.601	1.330	1.126	-	-	25.98
2155-304	2	0.117	0.320	0.272	-	-	24.89
2200+420	2	0.069	1.960	1.931	-	-	23.90
2254+074	1	0.190	-	-	-	-	-

Notes. This table contains information on the 45 BL Lac objects that are in either our sample or the Antonucci & Ulvestad (1985) sample. Columns are as follows. (1) Source name. (2) Sample ID: 1 = BL Lac contained in our sample or the Antonucci & Ulvestad (1985) sample that meets our first three selection criteria; 2 = BL Lac in the Antonucci & Ulvestad (1985) sample that does *not* meet our first three selection criteria. (3) Redshift. (4) Log(R_o) at 1.64 GHz. (5) Log(R_c) at 1.64 GHz. (6) Largest angular size (arcsec). (7) Largest linear size (kpc). (8) Log(L_{ext}), where L_{ext} = extended radio luminosity in W Hz^{-1} at 1.64 GHz.

The difference in redshift distributions between quasars and BL Lacs (Figs 4 and 5) is well known (for example, see Browne 1989). A consequence of this is that, although the R distributions are similar, the distributions of extended radio luminosity are very different (Fig. 6). These results suggest that quasars and BL Lacs have different statistical properties, and that their parent populations are also different. The difference between BL Lacs and quasars is further illustrated if we plot extended radio luminosity against redshift (Figs 7 and 8). The majority of the BL Lacs with measured redshifts and known extended emission have extended radio luminosity below the FRI/FRII luminosity division of $\approx 10^{25.4}$ W Hz^{-1} at 1.64 GHz, but this leaves a considerable number above this division and resurrects the issue of whether BL Lacs are beamed FRI radio galaxies. Some, or all, of the possibilities below may be true:

(1) BL Lacs know nothing about the FRI/FRII division and can be beamed versions of either type of radio source;

(2) the FRI/FRII division is blurred in luminosity, and the high-luminosity BL Lacs we see are in radio galaxies of FRI structure;

(3) some of the BL Lacs with $L_{ext} > 10^{25.4}$ W Hz^{-1} are misclassified and are really broad-line objects, i.e. they are quasars, and

(4) some of the objects have $L_{ext} > 10^{25.4}$ W Hz^{-1} by virtue of some beamed emission and are really FRIs.

We suspect that the third possibility is true, i.e. there are two types of objects that have been labelled as BL Lac objects, and some of the higher redshift 'BL Lacs' are really quasars. The hypothesis that genuine BL Lacs are beamed FRI radio galaxies is thus probably still tenable.

6.2 BL Lacs and microlensing

Our data are also relevant to the question of whether or not BL Lacs may be microlensed images of distant OVV/HPQ quasars (Ostriker & Vietri 1990). In Fig. 9, we show a plot of the largest angular size of the extended radio structure against redshift. In the microlensing picture this redshift would be that of the redshift of the galaxy in which lies the star producing the enhanced image of the HPQ core, and thus should be unrelated to the distance of the extended radio source. Contrary to the predictions of the lensing hypothesis, there is a clear trend for high-redshift sources to be smaller than low-redshift sources. This strongly suggests that the radio emission is at the distance indicated by the redshift and that microlensing is not the main reason why BL Lac objects have such singular properties. Moreover, in Sections 6.1 and 6.3 we show that the average R values of BL Lac objects are no higher than those of OVV/HPQ quasars. This is also inconsistent with the microlensing hypothesis, as it is only the core of the background OVV/HPQ which is gravitationally magnified and not the extended emission; the microlensed objects should therefore be very core-dominated.

6.3 Broad-line objects

Having seen that the BL Lac objects in our sample do not have higher values of R_o than the quasars, it is illustrative to divide the quasars (i.e. broad-line objects) into those known to be HPQs and those known not to be HPQs. Wills et al. (1992) report that there is a significant increase in the percentage of objects with high polarization (HPQs) with increasing R, which is in the expected sense for the unified

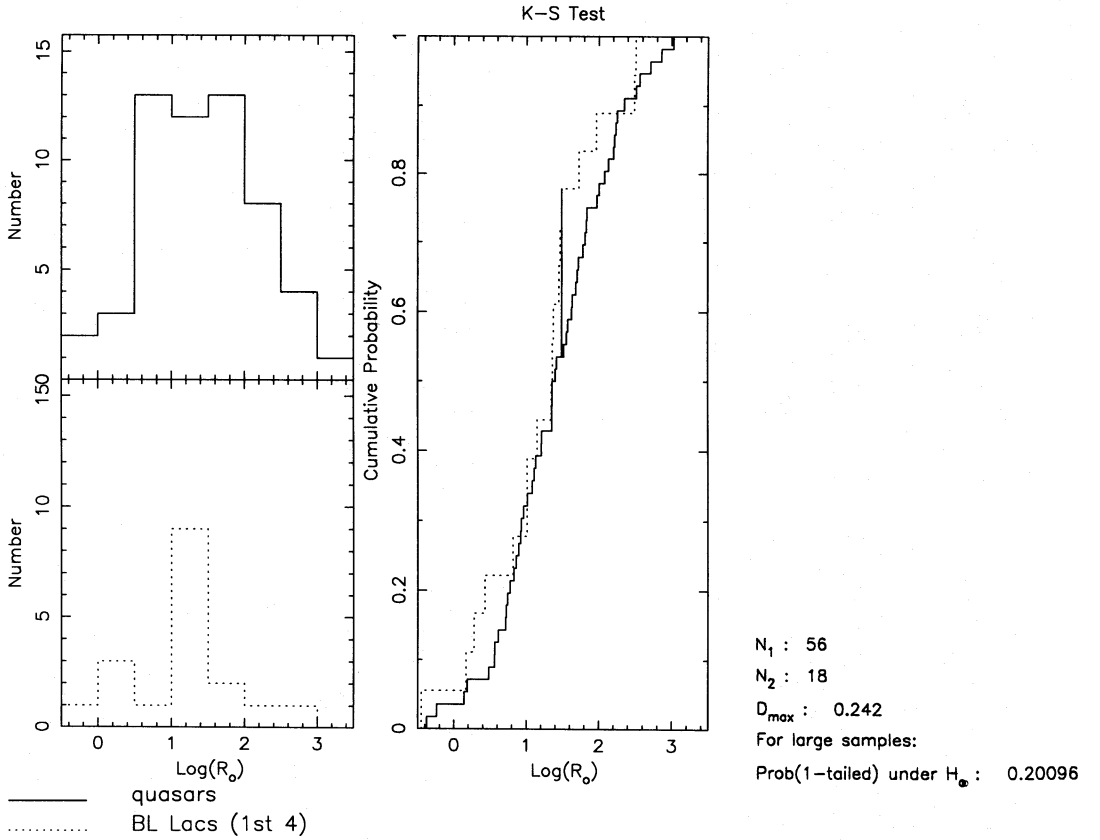

Figure 2. Histograms of $\log(R_o)$ for the 56/70 quasars in our sample and the 18/25 BL Lacs in the restricted sample for which extended emission is detected.

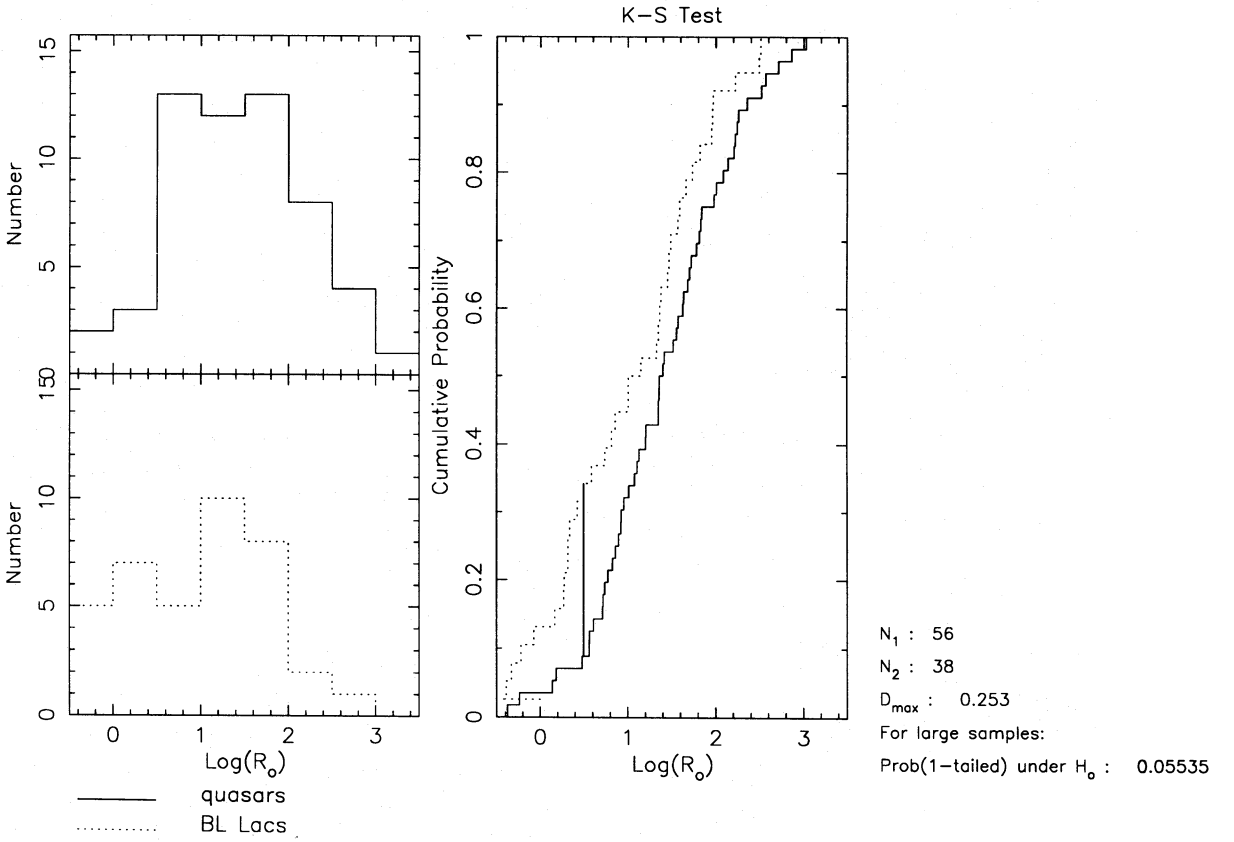

Figure 3. Histograms of $\log(R_o)$ for the 56/70 quasars in our sample and the 38/45 BL Lacs in the combined sample for which extended emission is detected.

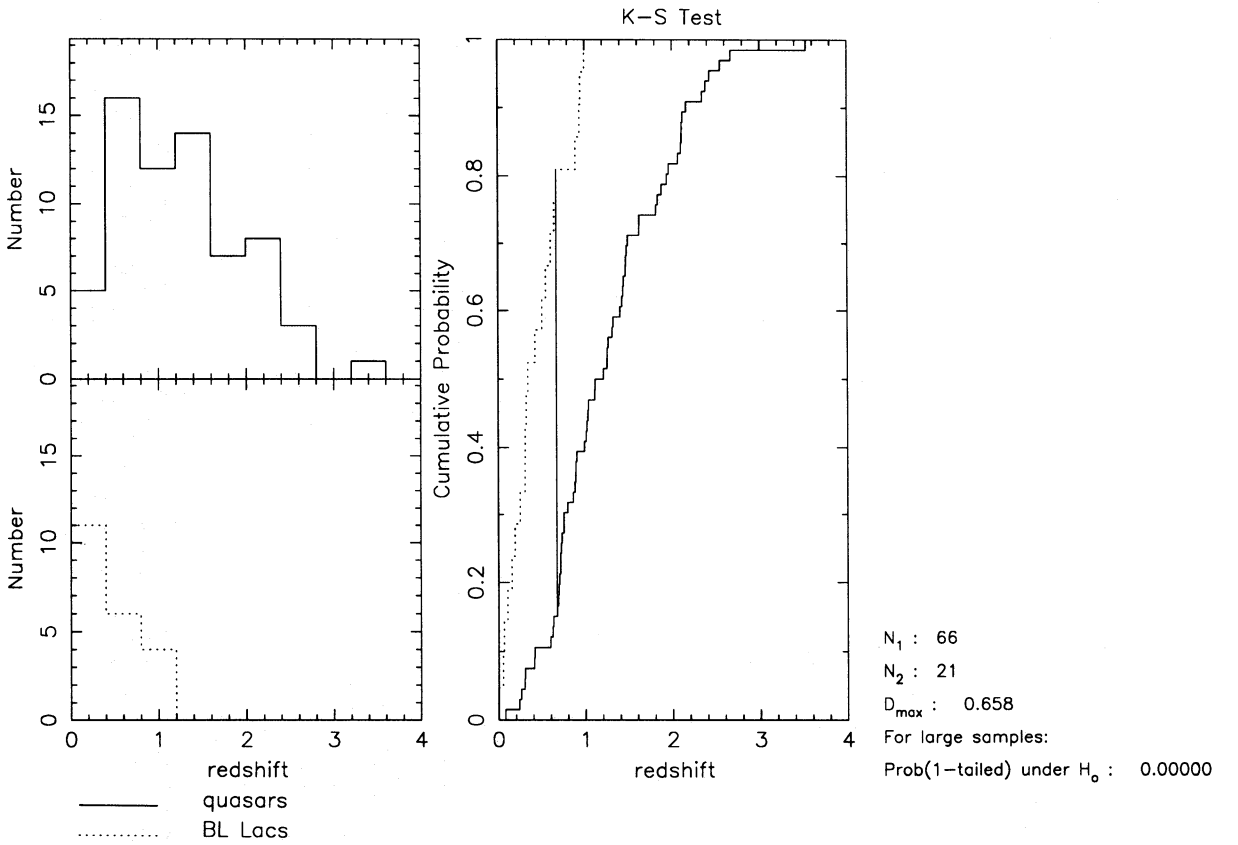

Figure 4. Redshift distributions of the 66/70 quasars in our sample and the 21/25 BL Lacs in the restricted sample that have measured redshifts.

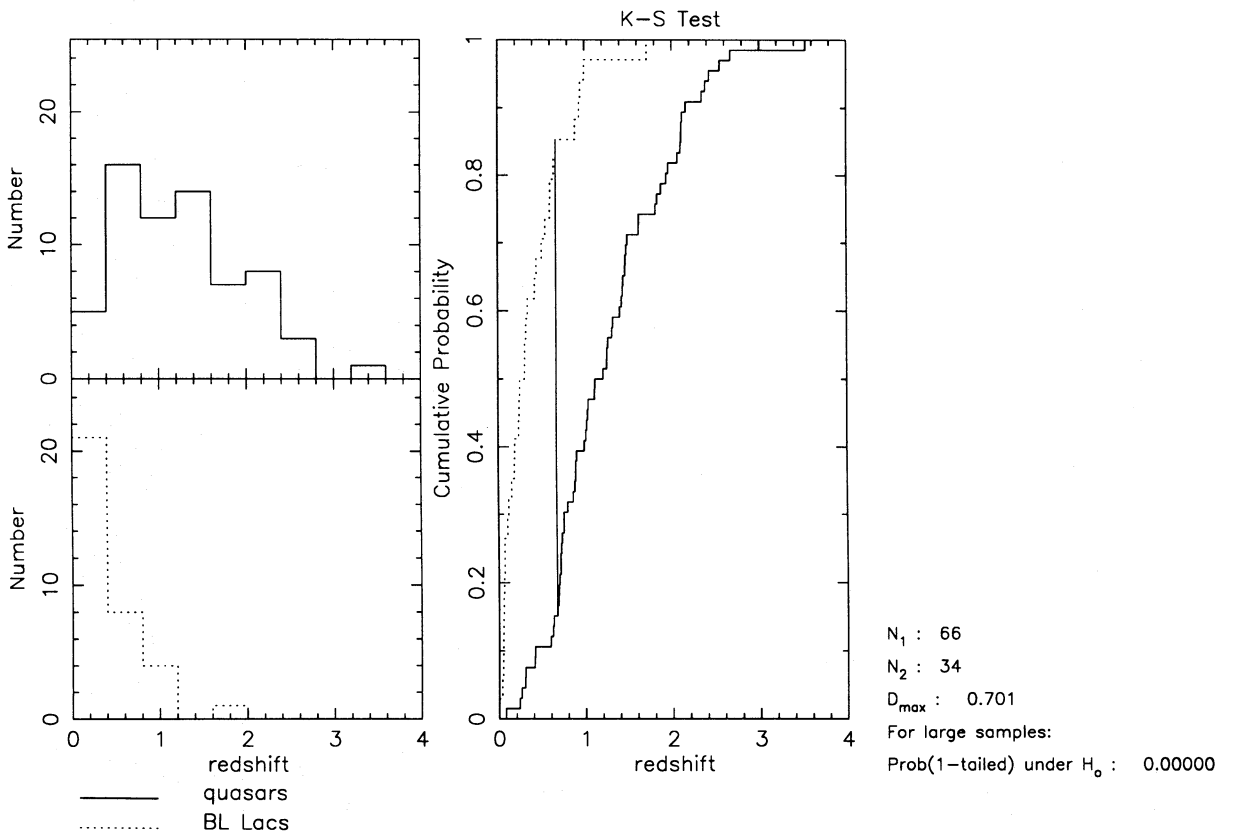

Figure 5. Redshift distributions of the 66/70 quasars in our sample and the 34/45 BL Lacs in the combined sample that have measured redshifts.

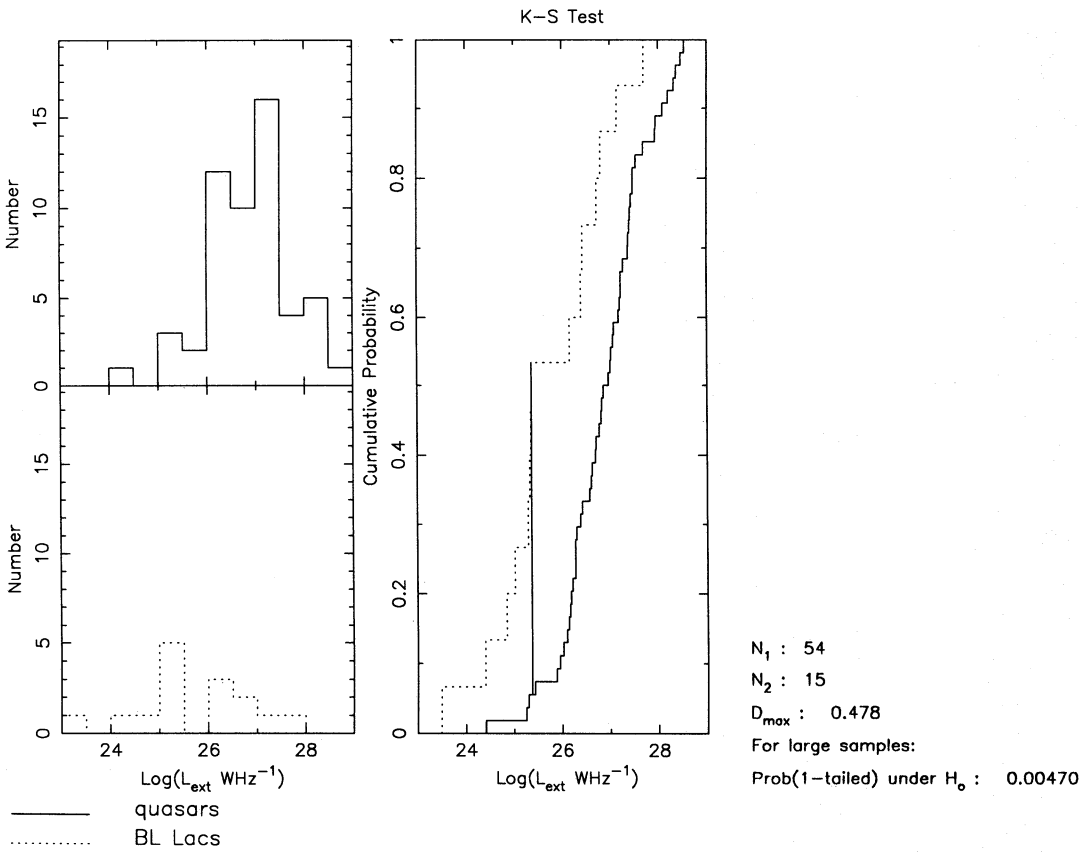

Figure 6. Extended radio luminosity distributions of the 54/70 quasars in our sample and the 15/25 BL Lacs in the restricted sample that have detected extended emission and measured redshifts.

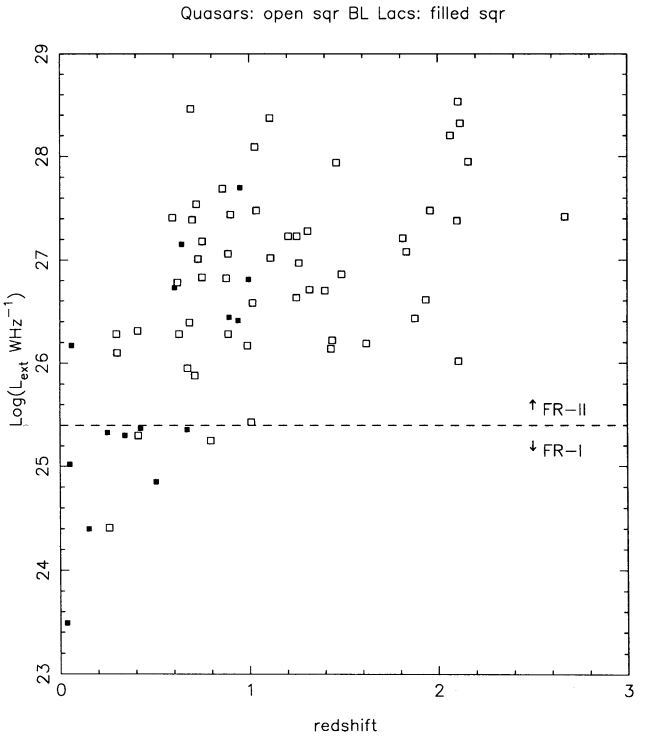

Figure 7. Graph of log (L_{ext}) against redshift for the 54/70 quasars in our sample (open squares) and the 15/25 BL Lacs in the restricted sample (filled squares) that have detected extended emission and measured redshifts.

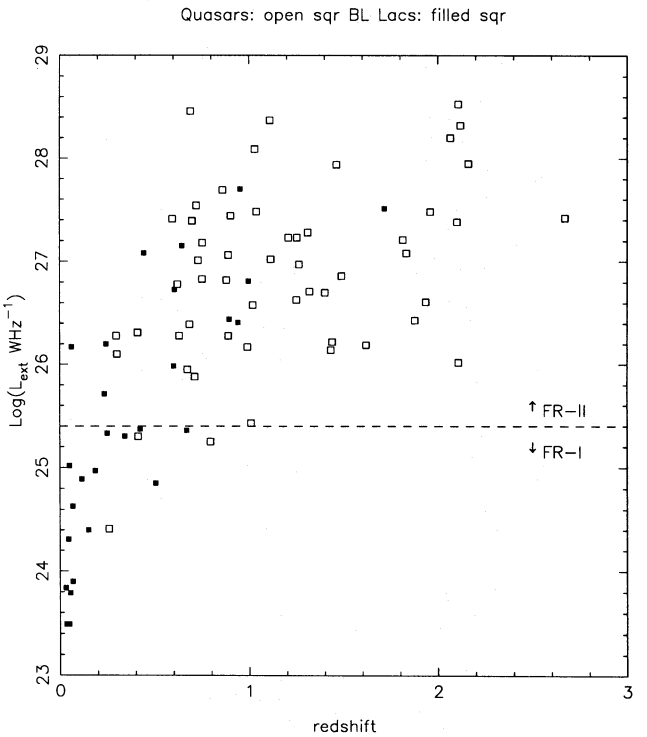

Figure 8. Graph of log (L_{ext}) against redshift for the 54/70 quasars (open squares) in our sample and the 28/45 BL Lacs (filled squares) in the combined sample that have detected extended emission and measured redshifts.

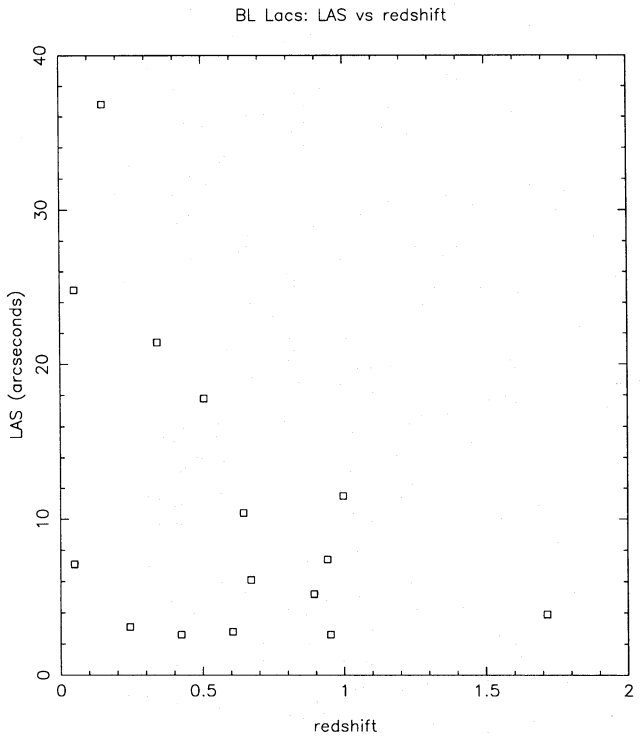

Figure 9. Graph of LAS against redshift for the 15/45 BL Lacs with measured redshifts and angular sizes.

sequence of Blandford & Königl (1979). In the sample of 55 quasars with polarization measurements, 21 are HPQs and the remaining 34 are non-HPQs. We have detected radio emission around 19/21 HPQs and 29/34 non-HPQs, and in Fig. 10 we plot the R_c distributions for both HPQs and non-HPQs. The Kolmogorov–Smirnov test shows that the two R_c distributions do not differ significantly. Thus we see no evidence for higher R values in the HPQs compared to the non-HPQs, evidence that would be expected if the HPQs were the same as the non-HPQs but viewed at smaller angles to the line of sight. However, this may indicate that all core-dominated quasars are inherently similar and periodically go through a state of blazar activity as suggested by Fugmann (1988).

In Fig. 11 we display our results in the same form as those of Wills et al. (1992). For our objects with polarimetry, we plot the fraction that are HPQs as a function of R_c. There is no tendency for this fraction to increase with R_c. Thus our results appear to disagree with the results of Wills et al., who show that the fraction of objects with blazar activity is a strong function of R, with nearly all high-R objects (>100) having high optical polarizations. Part of the reason for this disagreement is that Wills et al. include in their analysis quasars with very low R values, whereas our sample is limited to core-dominated objects most of which have $R>1$. Yet even among core-dominated objects the Wills et al. sample shows a strong correlation of the fraction of HPQs

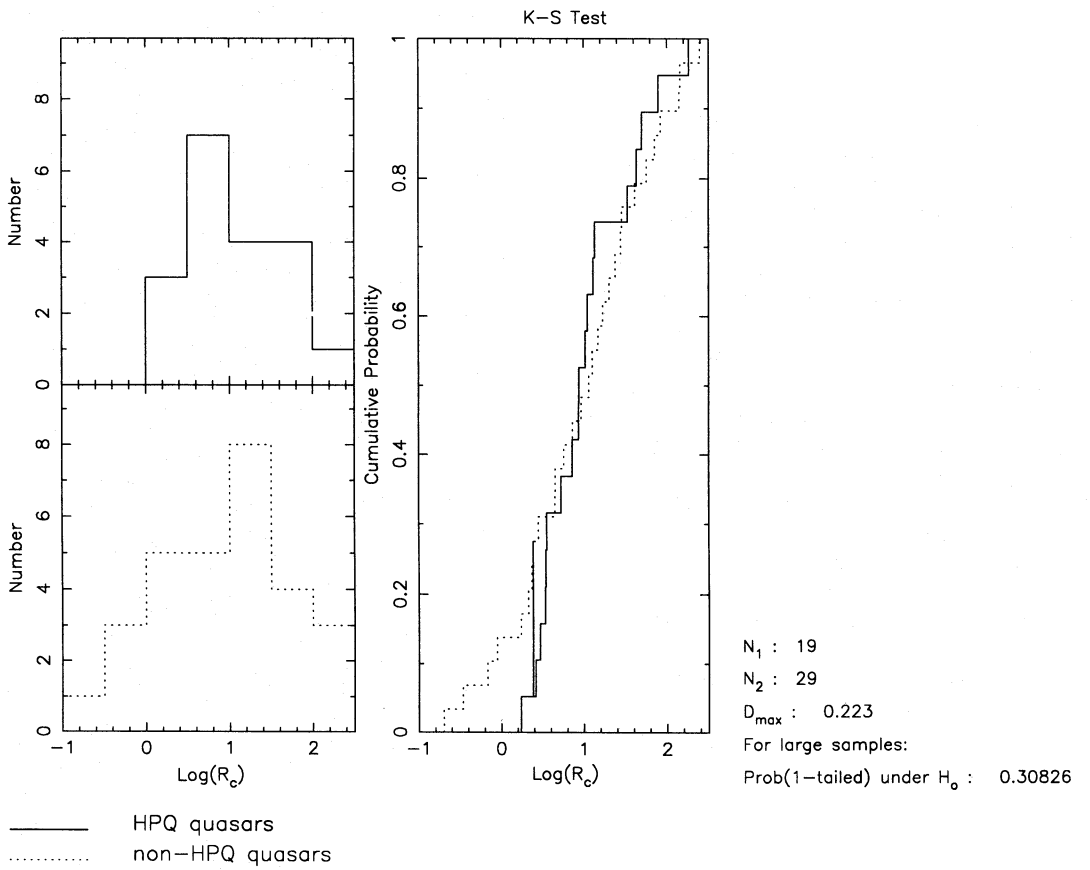

Figure 10. Log(R_c) distributions for the 19/21 HPQ quasars and the 29/34 non-HPQ quasars in our sample with detected extended emission and measured redshifts.

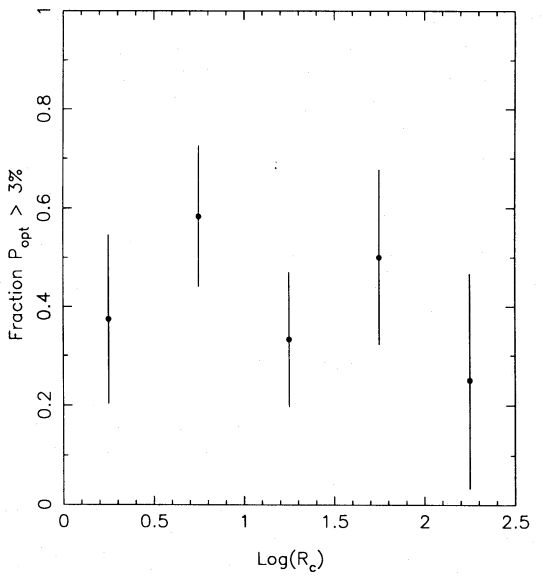

Figure 11. Fraction of the quasars in our sample with $R_c > 1$ classified either as HPQs or non-HPQs, with $P_{opt} > 3$ per cent as a function of log (R_c).

with R. There is no such trend for the quasars in our sample, nor is there a trend for those core-dominated quasars from the Wills et al. sample that overlap our sample. Clearly, the only way to resolve this disagreement is to increase the size of samples with optical polarimetry and with radio maps having high dynamic range.

7 CONCLUSIONS

We have shown that it is possible to make very high dynamic range VLA maps of strong sources with a series of very short observations. This enables us to detect low-brightness extended radio structure associated with highly core-dominated objects. We have used our data for BL Lac objects to show that the degree of radio core-dominance in BL Lac objects is indistinguishable from that in quasars. We conclude that the oft-quoted view that BL Lacs are just the most highly beamed quasars is not supported by the radio data. The redshift distributions of BL Lac objects are very different from those of quasars, hence the luminosity of the extended emission in most BL Lacs is more like those of low-luminosity (FRI) radio galaxies. The core-dominated quasars have extended radio luminosities typical of FRII radio galaxies and quasars (Paper II). Interestingly, a significant fraction of BL Lacs, especially those with redshifts > 0.5, have FRII extended radio luminosity. These FRII-luminosity BL Lacs are difficult to explain within the context of existing unified schemes, unless some 'BL Lacs' have been misclassified or some of the extended radio emission is beamed.

We also find that HPQs and non-HPQs have indistinguishable radio properties. This is surprising, since the most obvious interpretation is that HPQs have a stronger beamed synchrotron optical component and this would be expected to arise if the HPQs were being viewed at smaller angles to the line of sight than the average core-dominated quasar.

ACKNOWLEDGMENTS

Portions of this work were carried out at the Nuffield Radio Astronomy Laboratories while DWM held a SERC studentship, at NRAO as part of their summer student programme and at the Jet Propulsion Laboratory, California Institute of Technology, under contract with NASA. The National Radio Astronomy Observatory is operated by Associated Universities, Inc., under cooperative agreement with the NSF.

REFERENCES

Antonucci R. R. J., Ulvestad J. S., 1985, ApJ, 294, 158
Barthel P. D., 1989, ApJ, 336, 606
Blandford R. D., Königl A., 1979, ApJ, 232, 34
Blandford R. D., Rees M. J., 1978, in Wolfe A. M., ed., Pittsburgh Conference on BL Lac Objects. Univ. Pittsburgh, Pittsburgh, p. 328
Boroson T. A., 1992, ApJ, 399, L15
Browne I. W. A., 1983, MNRAS, 204, 23P
Browne I. W. A., 1989, in Maraschi L., Maccacaro T., Ulrich M.-H., eds, BL Lac Objects. Springer-Verlag, Berlin, p. 401
Browne I. W. A., Perley R. A., 1986. MNRAS, 222, 149
Burbidge G., Hewitt A., 1987, AJ, 92, 1
Cohen M. H., 1989, in Maraschi L., Maccacaro T., Ulrich M.-H., eds, BL Lac Objects. Springer-Verlag, Berlin, p. 13
Fugmann W., 1988, A&A, 205, 86
Heckman T. M., 1983, ApJ, 271, L5
Kristian J., Sandage A., 1970, ApJ, 162, 391
Kühr H., Schmidt G. D., 1990, AJ, 99, 1
Kühr H., Nauber U., Pauliny-Toth I. I. K., Witzel A., 1979, MPIfR Preprint # 55
Kühr H., Witzel A., Pauliny-Toth I. I. K., Nauber U., 1981, A&AS, 45, 367
Lawrence A., 1987, PASP, 99, 309
Orr M. J. L., Browne I. W. A., 1982, MNRAS, 200, 1067
Ostriker J. P., Vietri M., 1990, Nat, 344, 45
Peacock J. A., 1987, in W. Kundt, ed., Astrophysical Jets and their Engines. Reidel, Dordrecht, p. 185
Pearson T. J., Readhead A. C. S., 1988, ApJ, 328, 114
Perley R. A., 1989, in Perley R. A., Schwab F. R., Bridle A. H., eds, ASP Conf. Ser. 6, Synthesis Imaging in Radio Astronomy. Astron. Soc. Pac., San Francisco, p. 287
Scheuer P. A. G., 1987, in Zensus J. A., Pearson T. J., eds, Superluminal Radio Sources. Cambridge Univ. Press, p. 104
Schilizzi R. T., de Bruyn A. G., 1983, Nat, 303, 26
Stickel M., Padovani P., Urry C. M., Fried J. W., Kühr H., 1991, ApJ, 374, 431
Urry C. M., Padovani P., 1991, ApJ, 371, 60
Véron-Cetty M.-P., Véron P., 1991, A Catalogue of Quasars and Active Nuclei (5th edition). European Southern Observatory report No. 10, ESO, Garching
Wills B. J., Wills D., Breger M., Antonucci R. R. J., Barvainis R., 1992, ApJ, 398, 454